Submitted to ApJ
Preprint typeset using LaTeX style emulateapj v. 03/07/07

LYMAN-α EMITTERS AND LYMAN-BREAK GALAXIES AT $Z = 3-6$ IN COSMOLOGICAL SPH SIMULATIONS

Kentaro Nagamine[1], M. Ouchi[2,3], V. Springel[4], & Lars Hernquist[5]

Submitted to ApJ

ABSTRACT

We study the properties of Lyman-α emitters (LAEs) and Lyman-break galaxies (LBGs) at $z = 3-6$ using cosmological SPH simulations. We investigate two simple scenarios for explaining the observed Lyα and rest-frame UV luminosity functions (LFs) of LAEs: (i) the "*escape fraction*" scenario, in which the *effective* escape fraction (including the IGM attenuation) of Lyα photons is $f_{\rm Ly\alpha} \approx 0.1$ (0.15) at $z = 3$ (6), and (ii) the "*duty cycle*" scenario, in which the fraction of LAEs that are turned on at $z = 3$ (6) is $C_{\rm duty} \approx 0.07$ (0.2) after correcting for the IGM attenuation. Our comparisons with a number of different observations suggest that the duty cycle scenario is preferred over the escape fraction scenario. We find that the mean values of stellar mass, metallicity and black hole mass hosted by LAEs are all smaller in the duty cycle scenario than in the escape fraction scenario. In our simulations, the galaxy stellar mass function evolves rapidly, as expected in hierarchical structure formation. However, its evolution is largely compensated by a beginning decline in the specific star formation rate, resulting in little evolution of the rest-frame UV LF from $z = 6$ to 3. The rest-frame UV LF of both LAEs and LBGs at $z = 3$ & 6 can be described well by the duty cycle scenario provided the extinction is moderate, $E(B-V) \approx 0.15$, for both populations, although our simulation might be overpredicting the number of bright LBGs at $z = 6$. We show that the correlation function of LAEs in the duty cycle scenario has a smaller correlation length than in the escape fraction scenario. The bias of LAEs relative to the dark matter distribution is higher at $z = 6$ than at $z = 3$ in both scenarios. The Lyα LFs at $z = 6$ in a field-of-view of 0.2 deg^2 show a significantly larger scatter owing to cosmic variance relative to that in a 1 deg^2 field, and the scatter seen in the current observational estimates of the Lyα LF can be accounted for by cosmic variance.

Subject headings: cosmology: theory — stars: formation — galaxies: high-redshift — galaxies: evolution – galaxies: formation – methods: numerical

1. INTRODUCTION

Hydrogen is ubiquitous in our universe, and its Lyα emission line is now commonly observed in the spectra of high-z galaxies (e.g., Shapley et al. 2003; Ouchi et al. 2005b; Hu & Cowie 2006). Recent detections of LAEs in large numbers at $z = 3-6$ using narrow-band filters have opened up a new window for studying high-z galaxies after the long effort since the original proposal (Partridge & Peebles 1967) of using Lyα emission for the search of high-z galaxies.

In particular, wide-field surveys have been extremely successful in searching for LAEs, and the sizes of observed samples are becoming comparable to that of LBGs with several hundred sources (e.g., Ouchi et al. 2003a; Hu et al. 2004; Dawson et al. 2004; Malhotra & Rhoads 2004; Ouchi et al. 2005a; Taniguchi et al. 2005; Venemans et al. 2005; Shimasaku et al. 2006; Kashikawa et al. 2006; Gronwall et al. 2007; Murayama et al. 2007). These large samples allow us to construct the luminosity function (LF) of LAEs with reasonable accuracy and to perform statistical analyses and comparisons with other populations such as LBGs, DRGs, EROs, BzKs, etc.

At the same time, deep observations of smaller samples at infrared (IR) wavelengths are beginning to constrain the physical properties of LAEs such as stellar mass and star formation rate (SFR). For example, Gawiser et al. (2006) stacked the SEDs of 18 LAEs at $z \simeq 3.1$, and estimated an average stellar mass of $M_\star \simeq 5 \times 10^8\, h_{70}^{-2}\, M_\odot$ and a star formation rate of SFR $\simeq 6\, h_{70}^{-2}\, M_\odot\,{\rm yr}^{-1}$ by fitting the SED using a population synthesis model. Gawiser et al. (2007) updated the result using 162 LAEs from the MUSYC survey and reported $M_\star \simeq 1.0^{+0.6}_{-0.4} \times 10^9\, M_\odot$ and SFR $\simeq 2 \pm 1\, M_\odot\,{\rm yr}^{-1}$ for typical LAEs at $z = 3.1$. Lai et al. (2007b) analyzed the same sample of $z = 3.1$ LAEs supplemented by the Spitzer IRAC observations, and found $M_\star = 3^{+4}_{-2} \times 10^8\, M_\odot$, an age of $\sim 200\,$Myr, and an average SFR of $2\, M_\odot\,{\rm yr}^{-1}$ for the IRAC(3.6μm)-undetected sample. The IRAC-detected sample is more massive with $M_\star = 9 \pm 3 \times 10^9\, M_\odot$, age $= 1.6 \pm 0.4\,$Gyr, and SFR $\sim 6\, M_\odot\,{\rm yr}^{-1}$.

At higher redshifts, Pentericci et al. (2007) studied $z \sim 4$ LBGs with and without Lyα emission, and concluded that the LBGs with Lyα emission are on average much younger and less massive than the LBGs without Lyα emission. They estimated $M_\star = (5 \pm 1) \times 10^9 M_\odot$ and an age of $200 \pm 50\,$Myr for the LBGs with Lyα emission. Pirzkal et al. (2007) studied the SEDs of 9 LAEs in the Hubble Ultra Deep Field at $4.0 < z < 5.7$, and

[1] University of Nevada Las Vegas, Department of Physics & Astronomy, 4505 Maryland Pkwy, Box 454002, Las Vegas, NV 89154-4002 U.S.A.
[2] Observatories of the Carnegie Institution of Washington, 813 Santa Barbara Street, Pasadena, California, 91101 U.S.A.
[3] Carnegie Fellow
[4] Max-Planck-Institut für Astrophysik, Karl-Schwarzschild-Straße 1, 85740 Garching bei München, Germany
[5] Harvard University, 60 Garden Street, Cambridge, MA 02138, U.S.A.

estimated $M_\star = 10^6 - 10^8 M_\odot$ and SFR $\approx 8\,M_\odot\,\mathrm{yr}^{-1}$. Lai et al. (2007a) employed near-IR data of the *Spitzer* IRAC to increase the reliability of stellar mass estimates, and derived $M_\star = 10^9 - 10^{10}\,M_\odot$ and ages of $5 - 100\,\mathrm{Myr}$ using 3 LAEs at $z \sim 5.7$ in the GOODS northern field. Overall, these observations suggest that LAEs are in general less massive, have lower SFRs, and are younger than LBGs.

It has been suggested that LAEs might be exhibiting a very early phase of galaxy formation (e.g., Hu & McMahon 1996; Mori & Umemura 2006), where the Lyα photons emitted from the photoionized gas around star-forming regions are still able to escape from a relatively dust-free environment. However, it is also expected that Lyα emission might be observed from a later stage of galaxy formation (Shapley et al. 2003), because the galactic outflows driven by SNe can evacuate the dusty gas around star-forming regions, as observed in local starburst galaxies (Heckman 2001) and high-z LBGs (Pettini et al. 2001, 2002; Adelberger et al. 2003).

These ideas suggest evolutionary transitions from an early LAE to a LBG, and then back to a LAE at a later time. If this scenario is correct, then LAEs could be short-lived phenomena that occur only at certain phases of galaxy formation, and we need to consider the duty cycle of LAEs, similar to that of quasars (e.g., Haiman & Hui 2001).

Furthermore, Kashikawa et al. (2007) detected an interesting segregation between LBGs and LAEs around a high-z quasar, and proposed that the existence of LAEs might be suppressed by the intense UV radiation from the nearby quasar. This suggests that the existence of LAEs could be affected by various parameters of the local environment, such as overdensity or intensity of the UV radiation field.

Another interesting development in recent observations is that the LF in the rest-frame UV continuum *of LAEs* begins to be constrained at the same time, as well as the Lyα LF. This sets important additional constraints to the evolution of LAEs from $z = 6$ to 3, requiring the models to fit the UV LF of LAEs as well as the Lyα LF. The UV LFs of LBGs at $z = 3 - 6$ are being measured with increasing accuracy (e.g., Ouchi et al. 2004a; Yoshida et al. 2006; Oesch et al. 2007; Bouwens et al. 2007; Iwata et al. 2007), and the comparison between the UV LFs of LBGs and LAEs would give us information about the relationship between LBGs and LAEs, which is one of the key questions that is intensely studied in the field.

Motivated by these observations, there have been several theoretical studies of LAEs using semianalytic models of galaxy formation. Le Delliou et al. (2005, 2006) used the semianalytic model of Baugh et al. (2005) to show that the Lyα LF of LAEs at $z = 3$ can be explained if a uniform escape fraction of Lyα photon $f_{\rm esc} = 0.02$ is assumed. Kobayashi et al. (2007) used the semianalytic model of Nagashima et al. (2005) and introduced a variable escape fraction of Lyα photons owing to galactic wind feedback in high-z galaxies.

In this paper, we use cosmological hydrodynamic simulations of galaxy formation based on the concordance Λ cold dark matter (CDM) model to study the properties of LAEs, with a focus on the evolution of SFR, Lyα & UV LFs, stellar mass and clustering. Previously, Nagamine et al. (2004c) and Night et al. (2006) examined the properties of LBGs at $z = 3 - 6$ using the same set of cosmological simulations analyzed here, and showed that the rest-frame UV LF of LBGs can be explained reasonably well with moderate extinction. Building on top of our previous work on LBGs, here we discuss the relationship between LBGs and LAEs.

TABLE 1
Simulation Parameters

Run	$L_{\rm box}$	$N_{\rm p}$	$m_{\rm DM}$	$m_{\rm gas}$	ϵ
Q5	10.	2×324^3	2.12×10^6	3.26×10^5	1.23
Q6	10.	2×486^3	6.29×10^5	9.67×10^4	0.82
D5	33.75	2×324^3	8.15×10^7	1.26×10^7	4.17
G6	100.0	2×486^3	6.29×10^8	9.67×10^7	5.33

Note. — Simulations employed in this study. The initial number of gas particles is equal to that of dark matter particles, hence $\times 2$ for $N_{\rm P}$. the masses of dark matter and gas particles ($m_{\rm DM}$ and $m_{\rm gas}$) are given in units of $h^{-1}M_\odot$, respectively, and ϵ is the comoving gravitational softening length in units of $h^{-1}\,\mathrm{kpc}$. The value of ϵ is a measure of spatial resolution. All runs adopt our "strong" wind feedback model.

We have so far only discussed the point sources of Lyα emission, but there are also sources with extended Lyα emission, called "Lyα blobs" (Keel et al. 1999; Steidel et al. 2000; Matsuda et al. 2004). One of the possibilities is that the extended Lyα emission is powered by the release of gravitational potential energy as the baryons condense inside dark matter halos (Haiman et al. 2000; Fardal et al. 2001). Using the same series of simulations as in this paper, Furlanetto et al. (2005) considered the Lyα emission from diffuse IGM and the gas in halos around galaxies, which is powered by gravitational processes and photoionizing background radiation. They concluded that the Lyα emission from recombinations that follow the absorption of stellar ionizing photons (i.e., the Lyα emission associated with star formation) dominates the total Lyα photon production rate. Furthermore, Saito et al. (2007) found that the number density of Lyα blobs are only $10 - 20\%$ of the total LAE population. Therefore, in this paper, we focus on the Lyα emission associated with star formation and do not consider Lyα blobs. We concentrate on the comparison with updated observations of LAE LF and their relationship to those of LBGs.

This paper is organized as follows. In § 2, we briefly describe our simulations. We then discuss the specific SFR and stellar masses of high-z galaxies in our simulations in § 3. We present the evolution of the galaxy stellar mass function in § 4, and discuss the evolution of the Lyα LF from $z = 6$ to 3 in § 5. We propose two simple scenarios to explain the Lyα LF of LAEs. For both scenarios, we compute the mean values of stellar mass (§ 6), black hole masses (§ 7) and metallicity (§ 8) of LAEs. We discuss the relationship between Lyα and UV LFs in § 9, and their evolution in § 10. The correlation function of LAEs is presented in § 11. Finally, we discuss the cosmic variance in the current surveys of LAEs in § 12 and conclude in § 13.

2. SIMULATIONS

We use the smoothed particle hydrodynamics (SPH) code GADGET2 (Springel 2005) in this work. It employs the 'entropy conserving' formulation (Springel & Hernquist 2002) to alleviate the overcooling

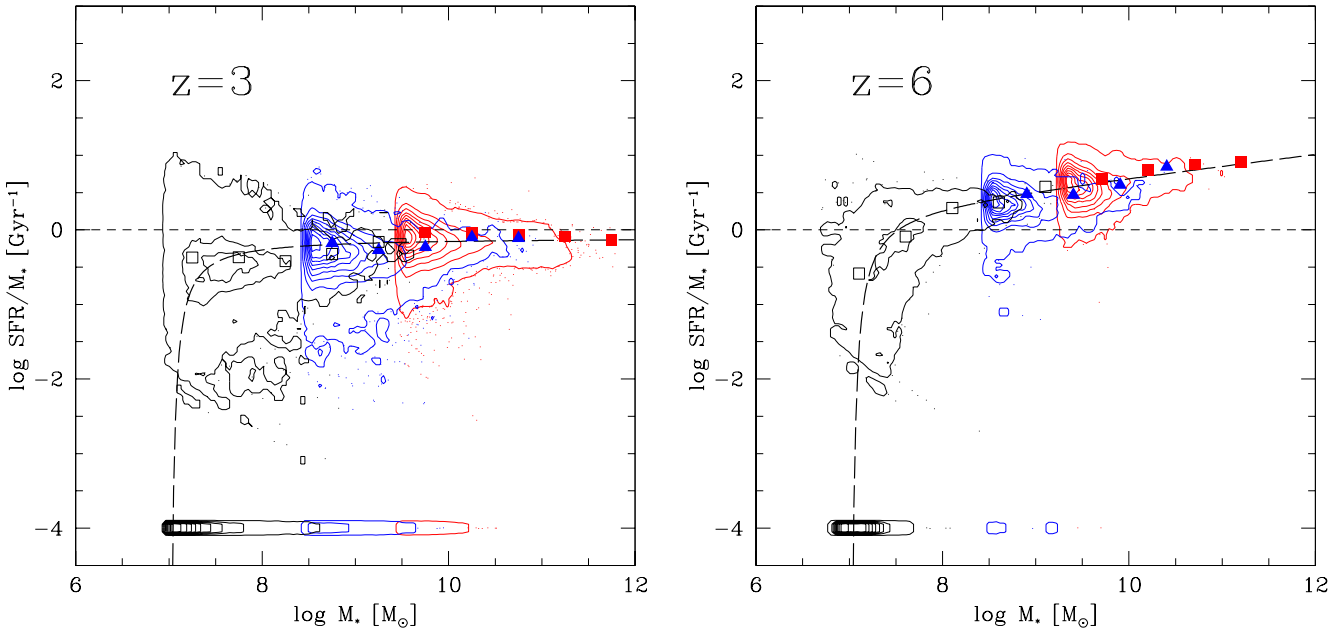

FIG. 1.— Specific star formation rate vs. galaxy stellar mass at $z = 3$ and 6. The three sets of contours are for the Q5 (black), D5 (blue) and G6 (red) run from left to right. The median in each mass bin is shown with the symbols. The analytic fits to the median points are shown with the long-dashed line and are given in the text. Galaxies with zero SFR are indicated at $\log \mathrm{SFR}/M_\star = -4$.

problem, which previous generations of SPH codes experienced. Our simulations include radiative cooling by hydrogen and helium, heating by a uniform UV background (e.g., Katz et al. 1996; Davé et al. 1999), star formation and supernova feedback based on a subparticle multiphase ISM model (Springel & Hernquist 2003a), and a phenomenological model for galactic winds (Springel & Hernquist 2003b).

The details of the star formation model were described in Nagamine et al. (2004b), so we only give a brief description here. In short, gas particles are allowed to spawn a new star particle when a set of criteria is satisfied at each time-step. Groups of star particles are regarded as galaxies in the simulation, and we identify them by apply a grouping algorithm. The code tags the star particles with physical quantities such as their mass, formation time, and metallicity. Using these tags, we compute the spectrum of each star particle with the population synthesis code of Bruzual & Charlot (2003), and co-add the individual luminosities to obtain the spectra of our simulated galaxies.

We use four different simulations with varying box sizes and particle numbers (see Table 1) in order to cover a wide range of halo masses and assess the resolution effect. These simulations extend the set of runs carried out by Springel & Hernquist (2003b) to higher resolution. Unfortunately, the Q6 simulation was stopped at $z \sim 4$ owing to its very long computing time. Therefore we basically use the Q5 run in this paper, and show the results from the Q6 run for $z = 6$ where appropriate. The results of the Q5 and Q6 runs are very similar at $z = 6$, except that the Q6 run has a slightly better coverage for the lowest mass galaxies with $M_\star \lesssim 10^{7.5}\,M_\odot$. The main conclusions of this paper are not affected by the absence of Q6 results at lower redshifts. The adopted cosmological parameters of all simulations considered here are $(\Omega_\mathrm{m}, \Omega_\Lambda, \Omega_\mathrm{b}, \sigma_8, h) = (0.3, 0.7, 0.04, 0.9, 0.7)$, where $h = H_0/(100\,\mathrm{km\,s^{-1}\,Mpc^{-1}})$.

3. SPECIFIC SFR AND GALAXY STELLAR MASS

We start by examining the instantaneous SFR of simulated galaxies at $z = 3$ and $z = 6$, because we will use this quantity to calculate the Lyα luminosity. Figure 1 shows the specific SFR ($\equiv \mathrm{SFR}/M_\star$; SFR per unit stellar mass) as a function of galaxy stellar mass at $z = 3$ and 6. The three sets of contours are for the Q5 (black), D5 (blue) and G6 (red) runs, from left to right. The Q6 result at $z = 6$ is very similar to that of Q5, so it is not shown here. Each simulation box can resolve only a limited range of galaxy masses, so we use three different simulations to cover a wide range of stellar masses, $M_\star = 10^7 - 10^{12}\,M_\odot$. The median value of the specific SFR is shown by the symbols for each bin of $\log M_\star$. The number of galaxies with no star formation is greater at $z = 3$ than at $z = 6$, as indicated at $\log \mathrm{SFR}/M_\star = -4.0$.

The distribution broadens at the lower mass end of each contour for two reasons. One is that there is a larger number of lower mass halos, therefore the distribution naturally becomes broader as the larger population exhibits a larger variation in its properties. The other reason is that the resolution limit of each run progressively shifts to lower masses, and close to the resolution limit the distribution broadens owing to numerical noise.

At $z = 3$, the specific SFR is almost constant (with significant scatter around the mean) across the mass range of $M_\star = 10^{8-10}\,M_\odot$. On the other hand, at $z = 6$, the specific SFR is an increasing function of galaxy stellar mass, indicating that star formation is more efficient in more massive galaxies. Star formation becomes rapidly inefficient in low mass galaxies with $M_\star < 10^8 M_\odot$, and the distribution seems to drop off completely at $M_\star \simeq 10^7 M_\odot$. This rapid fall-off of the SFR at $M_\star \simeq 10^7 M_\odot$ may be related to the threshold density for star formation in the simulation and the observed SF cutoff in nearby spiral galaxies (Kennicutt 1998). A detailed investigation of the SF threshold in the simulation is beyond the

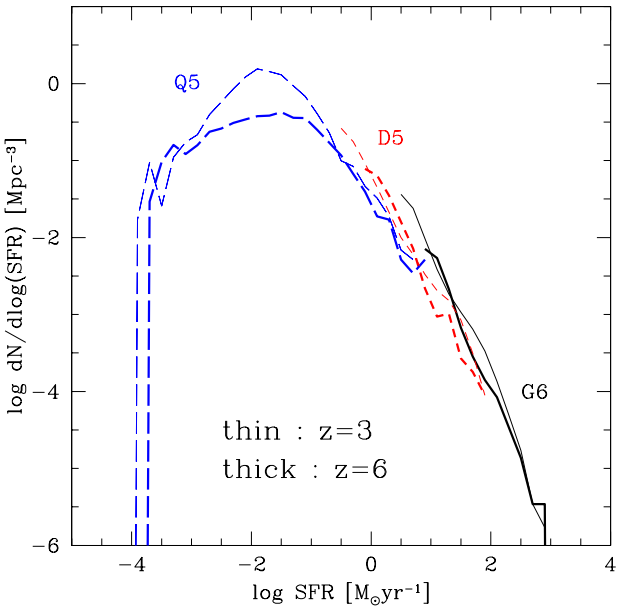

FIG. 2.— SFR function at $z = 3$ (thin lines) and $z = 6$ (thick lines) for the Q5 (long dashed), D5 (short dashed), and G6 (solid) runs.

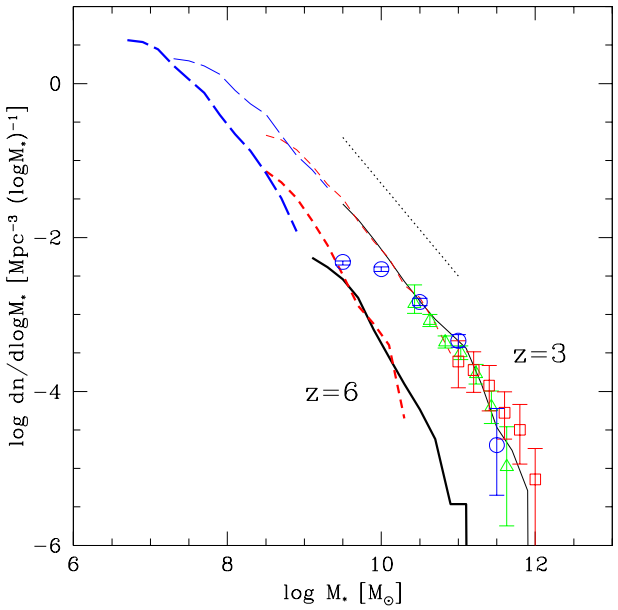

FIG. 3.— Galaxy stellar mass function at $z = 3$ (thin lines) and $z = 6$ (thick lines) for Q5 (long dashed; Q6 for $z = 6$), D5 (short dashed), and G6 (solid lines) runs. The dotted line indicates the power-law of $n(M_\star) \propto M_\star^{-2.2}$. The data points are from Drory et al. (2005, blue circles), Fontana et al. (2006, green triangles) and Perez-Gonzalez et al. (2007, red squares).

scope of this paper, and is deferred to future work.

We provide the following approximate fit to the median points shown in Fig. 1:

$$Y = aX - \frac{b}{X - c} + d, \tag{1}$$

where $(X, Y) = (\log M_\star, \log \mathrm{SFR}/M_\star)$, and $(a, b, c, d) = (0.0, 0.17, 7.0, -0.10)$ & $(0.15, 0.2, 7.0, -0.75)$ for $z = 3$ & 6, respectively. At $z = 3$, the down-turn at $\log M_\star \approx 7.0$ is not clearly seen, but we kept the value of c the same for both redshifts for simplicity.

Figure 2 shows the galaxy SFR function at $z = 3$ and 6, which measures the differential number density of galaxies per logarithmic bin of SFR, similarly to a galaxy luminosity function. We find that there is not much evolution in the SFR function from $z = 6$ to 3. This might seem counter-intuitive given the evolution seen in the specific SFR, however, the evolution of the SFR function is caused by a combined evolution in both the specific SFR and galaxy stellar mass functions.

4. GALAXY STELLAR MASS FUNCTION

In our simulations, the galaxy stellar mass function evolves rapidly from $z = 6$ to $z = 3$, as expected in a hierarchical universe (Figure 3); new halos of low mass are constantly formed, less massive galaxies merge into more massive systems, and the number density of massive galaxies increases with decreasing redshift. We note that galaxies grow in stellar mass in our simulations, but the star formation becomes less efficient from $z = 6$ to 3 (Fig. 1). The latter effect compensates for the growth of the mass function, resulting in little change in the SFR function (Fig. 2).

At $z = 3$, the simulation agrees well with the data from Drory et al. (2005, blue circles, $3.0 < z < 4.0$), Fontana et al. (2006, green triangles, $2.5 < z \leq 3.0$) and Perez-Gonzalez et al. (2007, red squares, $3.0 \leq z < 3.5$) at $\log M_\star \gtrsim 10.5$. The data by Drory et al. (2005) suggest that the mass function becomes shallower at $\log M_\star < 10.0$, but our simulations have a steeper slope ($n(M_\star) \propto M_\star^{-2.2}$) at the low-mass end as indicated by the dotted line. While it appears likely that our simulations overpredict the number of low-mass galaxies, future deeper observations are needed to check this, based on a more reliable measurement of the faint-end of the mass function. The location of the "knee" in the simulated mass function is uncertain, given the steep faint-end slope.

We compute the total stellar mass density by integrating the interpolated mass function in Fig. 3 over the mass range of $\log M_\star \approx [7.0, 12.0]$, and obtain $\rho_\star = 3.5 \times 10^8$ (8.8×10^7) $M_\odot\,\mathrm{Mpc}^{-3}$ at $z = 3$ (6). This corresponds to $\Omega_\star = 0.0026$ (6.5×10^{-4}) at $z = 3$ (6). These values are higher than any of the cosmic SFR models presented by Nagamine et al. (2006b, Fig. 6a), suggesting that the faint-end slope in Fig. 3 might be too steep. Nevertheless, we will use these total stellar mass densities in § 6 to compute the fraction of stellar mass that LAEs contribute.

5. Lyα LUMINOSITY FUNCTION

We compute the intrinsic Lyα luminosity $L_{\mathrm{Ly}\alpha}^{\mathrm{int}}$ emitted by high-z galaxies as

$$L_{\mathrm{Ly}\alpha}^{\mathrm{int}} = 10^{42}\,(\mathrm{SFR}/M_\odot\,\mathrm{yr}^{-1})\ \mathrm{erg\,s}^{-1}, \tag{2}$$

following Furlanetto et al. (2005). This relationship is accurate to within a factor of a few according to the stellar population synthesis model of Leitherer et al. (1999) for a Salpeter initial mass function (IMF) with a mass range of $1 - 100\,M_\odot$ and metallicities between $0.05 < Z/Z_\odot < 2$. We use the simulated SFR in the right-hand-side of Eq. (2).

Without any corrections to the Lyα luminosity, we find that our simulations overpredict the Lyα LF by a significant factor (~ 10) compared to the observations of Ouchi et al. (2007). Here, we choose to compare our results with the data by Ouchi et al. (2007), because their sample comes from a large survey field and they have performed extensive comparisons with the earlier LF estimates. Ouchi et al.'s LF at $z \sim 3$ is consistent with that of Gronwall et al. (2007). According to their data, there is not much evolution (no more than a factor of $2-3$) between $z = 6$ and 3 in the observed *apparent* Lyα LF either in luminosity or number density. However, Lyα fluxes from high-z sources are attenuated by the intergalactic neutral hydrogen, causing an asymmetric profile in the Lyα emission line with the blue-side being absorbed more (e.g., Hu et al. 2004; Kashikawa et al. 2006; Shimasaku et al. 2006). Therefore, when the data is corrected for this effect, little evolution in the *apparent* Lyα LF means strong evolution in the *intrinsic* LF, in the sense that the Lyα luminosity and/or the number density of LAEs are intrinsically brighter/higher at $z \simeq 6$ than at $z \simeq 3$.

In the following, we consider two possible scenarios to match the simulation results to the observed *apparent* Lyα LF. The two proposed scenarios are very simple, but they capture the two extreme situations that plausibly bracket the true behavior.

5.1. *Escape Fraction Scenario*

In the first scenario we simply assume that only a fixed fraction of Lyα photons reaches us from the source, i.e.,

$$F_{\rm Ly\alpha}^{\rm obs} = f_{\rm Ly\alpha} F_{\rm Ly\alpha}^{\rm intrinsic}, \tag{3}$$

where $F_{\rm Ly\alpha}$ is the Lyα flux. The parameter $f_{\rm Ly\alpha}$ can be interpreted as an *effective escape fraction* that includes the following three effects: escape of ionizing photons, local dust extinction, and absorption by the IGM (Barton et al. 2004). We characterize this as

$$f_{\rm Ly\alpha} = f_{\rm dust}\,(1 - f_{\rm esc}^{\rm ion})\,f_{\rm IGM}, \tag{4}$$

where $f_{\rm dust}$ is the fraction of Lyα photons that is *not* extinguished by local dust, $f_{\rm esc}^{\rm ion}$ is the fraction of ionizing photons that escape from galaxies and thus create no Lyα photons, and $f_{\rm IGM}$ is the fraction of Lyα photons that are *not* absorbed by the IGM, i.e., the transmitted flux. We call this case the "*escape fraction*" scenario.

Of course, in the real universe, different galaxies may have different values of $f_{\rm dust}$ and $f_{\rm esc}^{\rm ion}$, depending on their physical parameters such as age, mass, SFR and local environment. These parameters can also depend on redshift. Therefore, the above parameterization should be interpreted as an attempt to capture the *average* behavior of bright galaxies that are currently being observed, even though for simplicity we do not indicate the implicit averaging with $\langle\cdots\rangle$ in our notation.

The left column of Figure 4 shows a comparison of our simulation results with the observational data by Ouchi et al. (2007), adopting $f_{\rm Ly\alpha} = 0.1$ (0.15) for $z = 3$ (6). This scenario corresponds to simply shifting the simulated LF toward lower luminosity, therefore the currently observed LAEs correspond to relatively massive galaxies with high SFR. Here we selected the values of $f_{\rm Ly\alpha}$ such that the G6 run agrees well with the observed data points, because this run has the largest box size and covers the bright-end of the observed LF much better than our other runs. The D5 run underestimates the number density of massive galaxies with $\log L_{\rm Ly\alpha} \gtrsim 42$ owing to its smaller box size. The agreement between the simulation results and the observed data is very good at both $z = 3$ and 6, including the slope of the LF. Since our SFR function does not evolve very much (Fig. 2), the values of $f_{\rm Ly\alpha}$ at $z = 3$ and 6 are very close.

5.1.1. *5.1.1. IGM attenuation and $f_{\rm esc}^{\rm ion}$, $f_{\rm dust}$*

We estimate the effect of IGM attenuation to be

$$f_{\rm IGM} = e^{-\tau_{\rm eff}} = 0.82\ (0.52)\ \text{ for } z = 3\ (6) \tag{5}$$

using the Madau (1995) formulation with the assumption that only half of the symmetric Lyα line is absorbed. These values are consistent with those obtained by Ouchi et al. (2007). Inserting Eq. (5) into Eq. (4), we obtain

$$f_{\rm dust}\,(1 - f_{\rm esc}^{\rm ion}) = 0.12\ (0.29) \quad \text{for } z = 3\ (6). \tag{6}$$

Chen et al. (2007) reported that, using the afterglow spectra of long-duration gamma-ray bursts, the mean escape fraction of ionizing radiation from sub-L_* galaxies at $z \gtrsim 2$ is $\langle f_{\rm esc}^{\rm ion}\rangle = 0.02 \pm 0.02$ with an upper limit of $\langle f_{\rm esc}^{\rm ion}\rangle \le 0.075$. If the escape fraction of ionizing photons is as small as $f_{\rm esc}^{\rm ion} = 0.02$, then our result implies $f_{\rm dust} \approx 0.12$ (0.29) at $z = 3$ (6).

Inoue et al. (2006, Fig. 3) compiled existing direct measurements of escape fractions of ionizing photons and estimates based on the observed ionizing background intensities. They suggested that the value of $f_{\rm esc}^{\rm ion}$ might be increasing with redshift: $f_{\rm esc}^{\rm ion} \approx 0.02, 0.06$ & 0.2 at $z = 2, 3$ & $4-6$. In this case,

$$f_{\rm dust} = 0.13\ (0.36) \quad \text{at } z = 3\ (6). \tag{7}$$

The lower value of $f_{\rm dust}$ at $z = 3$ suggests that the environment around the star-forming regions becomes more polluted by dust as star-formation proceeds from $z = 6$ to 3, blocking more Lyα photons.

Many researchers (e.g., Le Delliou et al. 2006; Kobayashi et al. 2007) simply adopted $f_{\rm IGM} = 1.0$, arguing that various effects can reduce the amount of IGM attenuation, such as ionization of the IGM around galaxies, clearing of the IGM by galactic winds, and redshifting of Lyα photons by the scattering in the wind. They also refer to the fact that the reionization of the Universe was mostly completed by $z \sim 6$, as indicated by measurements of Gunn-Peterson absorption in quasar spectra, and as suggested by constraints on the clustering of LAEs (McQuinn et al. 2007). It is possible that the asymmetric Lyα line profile is caused by the local ISM at the source, rather than by the IGM. Given the large uncertainty in the value of $f_{\rm IGM}$, we also consider the case of $f_{\rm IGM} = 1.0$. In this case, our result implies $f_{\rm dust}\,(1 - f_{\rm esc}^{\rm ion}) = 0.10$ (0.15) for $z = 3$ (6). Adopting the values of $f_{\rm esc}^{\rm ion} = 0.06$ (0.20) at $z = 3$ (6) from Inoue et al. (2006), we obtain

$$f_{\rm dust} = 0.11\ (0.19) \quad \text{at } z = 3\ (6). \tag{8}$$

In either case, our results imply $f_{\rm dust} \approx 0.1$ at $z = 3$, and $f_{\rm dust} \approx 0.2 - 0.4$ at $z = 6$.

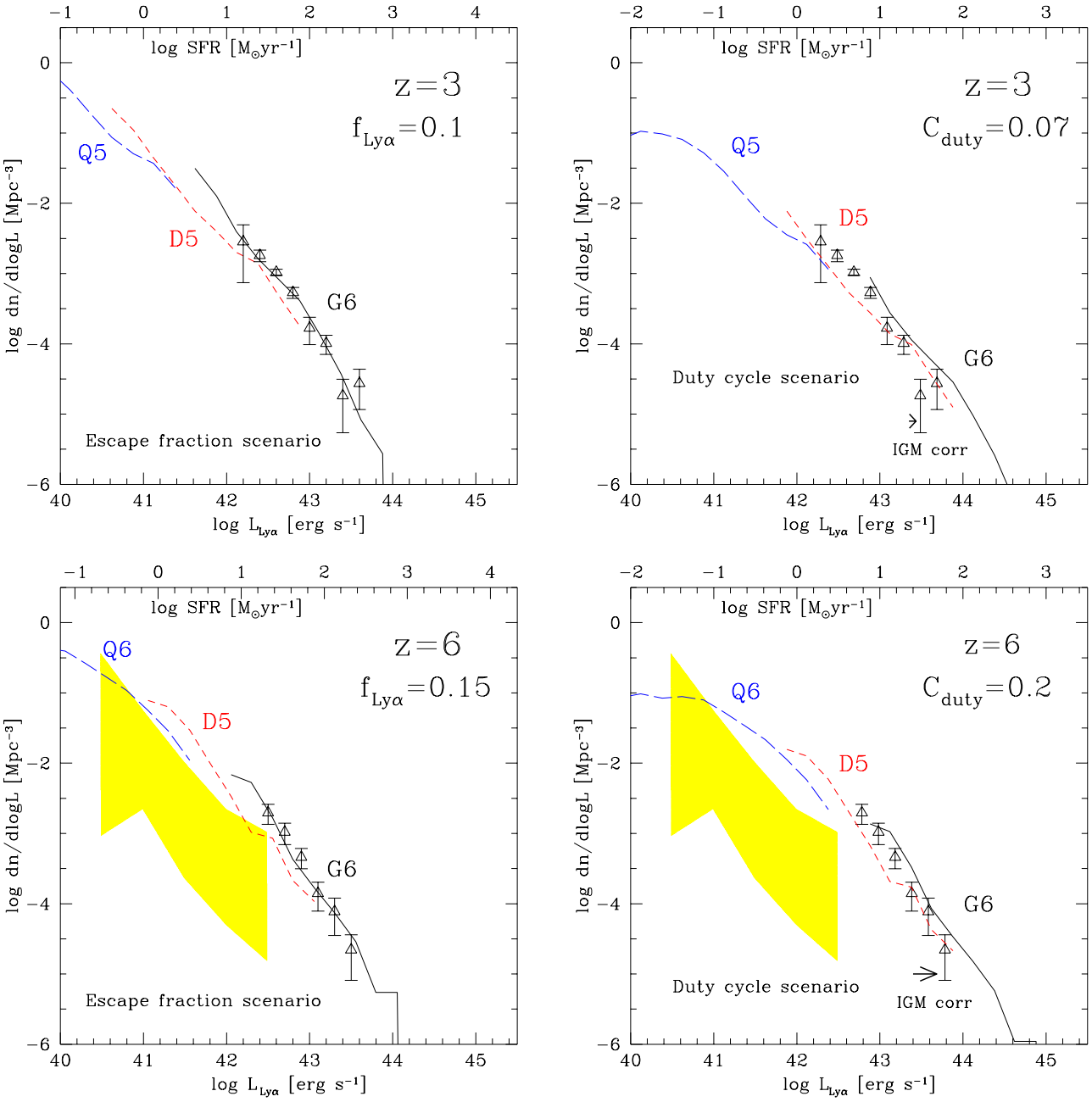

FIG. 4.— Lyα LF of LAEs at $z = 3$ (top row) and $z = 6$ (bottom row). The data points are from Ouchi et al. (2007) at $z = 3.1$ and $z = 5.7$. The left column is for the "*escape fraction*" scenario, and the right column is for the "*duty cycle*" scenario. In the right column panels, corrections of $(f_{\rm IGM})^{-1} = (0.82)^{-1}$ & $(0.52)^{-1}$ are applied to the data points of Ouchi et al. (2007) at $z = 3$ & 6, respectively. The IGM attenuation as indicated by the small arrows. The yellow shade in the bottom two panels indicates the region covered by the data points of Santos et al. (2004) and the simulation results of Davé et al. (2006).

5.2. *Duty Cycle Scenario*

The other scenario we examine is based on the assumption that only a fixed fraction ($C_{\rm duty}$) of all galaxies is active as LAEs at a given time. As far as the luminosity function is concerned, this is equivalent to assuming that each LAE has a certain duty cycle and remains turned on only for a fixed duration of time, therefore, we call this case the "*duty cycle*" scenario.

Before we calculate the values of $C_{\rm duty}$, we correct the observed Lyα LF for the effect of IGM attenuation by factors of $(f_{\rm IGM})^{-1} = (0.82)^{-1}$ & $(0.52)^{-1}$ for $z = 3$ & 6, respectively. As shown in the right column of Figure 4, we obtain good agreement with the data if we assume $C_{\rm duty} \approx 0.07$ (0.2) for $z = 3$ (6). This is equivalent to lowering the normalization of the simulated LF to match the observed data. Here we adjust our simulated LF so that the results of the D5 and G6 runs bracket the observed data points, because in this scenario the observed data overlaps with lower mass galaxies in the D5 run. The above value of $C_{\rm duty}$ can be interpreted as either only 7% of the sources are turned on as LAEs at $z = 3$, or LAEs are turned on only for 70 Myrs out of 1 Gyr at $z \approx 3$.

The yellow shaded region in the lower panels of Fig-

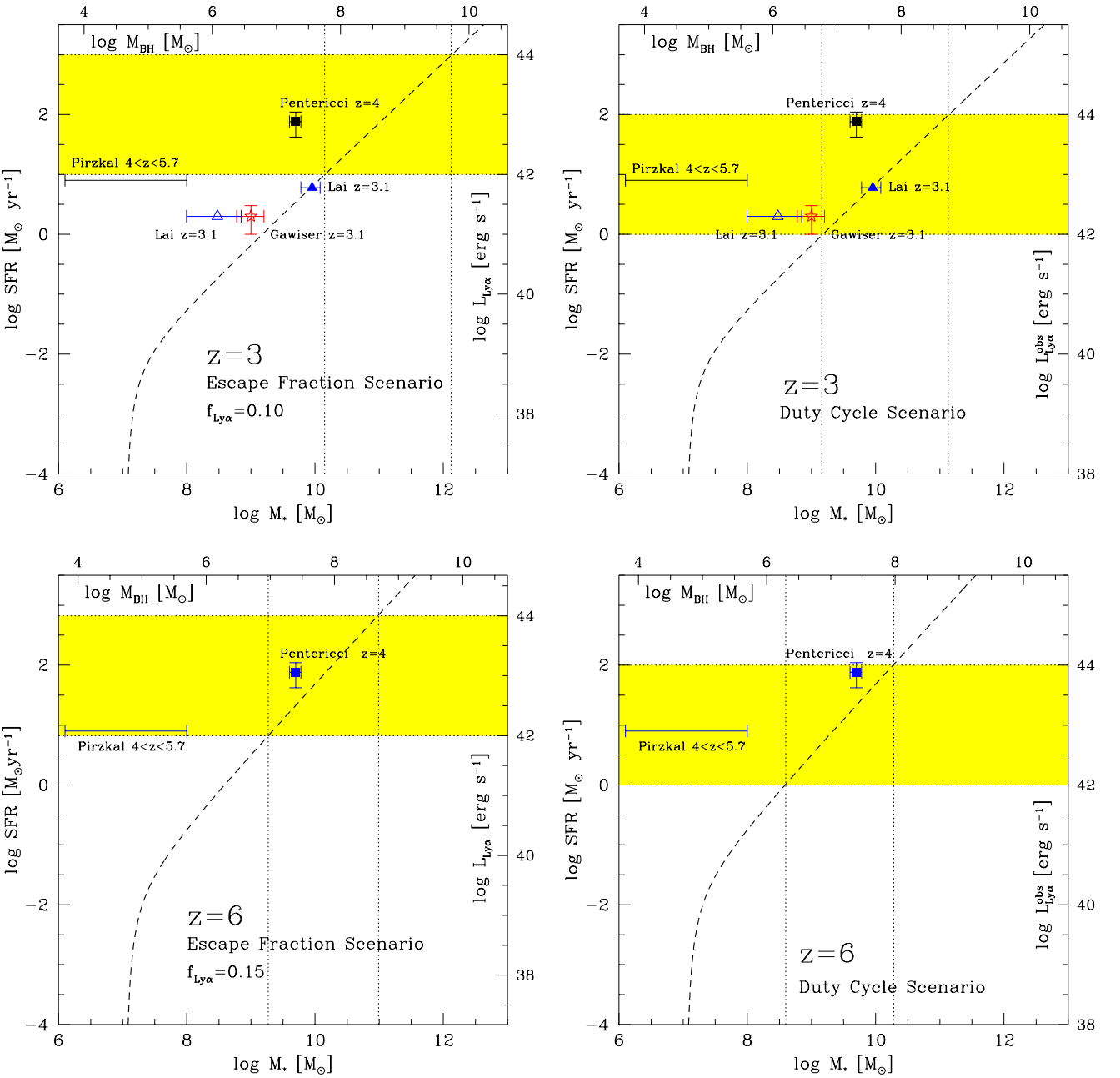

FIG. 5.— Summary of relationships between galaxy stellar mass, SFR, Lyα luminosity and BH mass assuming a ratio of $M_{\rm BH}/M_\star \approx 0.004$ (0.005) at $z = 3$ (6) (Hopkins et al. 2007c). The dashed lines are based on Eq. (1). The yellow shaded regions indicate the currently observed luminosity range of $\log L_{{\rm Ly}\alpha} = [42, 44]$. Data points are from Gawiser et al. (2007, open star), Lai et al. (2007b, open and filled triangles for IRAC-undetected and detected sample, respectively), Pentericci et al. (2007, filled square), and Pirzkal et al. (2007).

ure 4 indicates the region covered by the data points of Santos et al. (2004) and the simulation results of Davé et al. (2006). Their results are significantly lower than our simulation results at $\log L_{{\rm Ly}\alpha} = [40.5, 42.5]$. We comment further on this point in § 12 and § 13.

6. STELLAR MASS OF LAES

Figure 5 summarizes the relationship between galaxy stellar mass, SFR and Lyα luminosity. The yellow shaded regions indicate the luminosity range of $\log L_{{\rm Ly}\alpha} = [42, 44]$, which roughly corresponds to the currently observed LAEs at $z = 3-6$ (Ouchi et al. 2007). The corresponding stellar mass ranges differ significantly, depending on the two scenarios and redshift as summarized in Table 2, but they are not affected by the uncertainties in the value of $f_{\rm IGM}$, because Fig. 5 is solely determined by Eq. (2) and the values of $f_{{\rm Ly}\alpha}$.

In the escape fraction scenario, the raw (i.e., before any corrections) simulated Lyα LF is simply shifted toward lower luminosity without a change in the normalization, therefore currently observed LAEs correspond to the most massive and luminous objects at the brightest end of the LF. The mean stellar masses of LAEs with $\log L_{{\rm Ly}\alpha} = [42, 44]$ in the G6 run are

$$\langle M_\star \rangle = 2.5 \times 10^{10}\ (1.9 \times 10^9)\, M_\odot \text{ at } z = 3\ (6), \quad (9)$$

respectively, as given in Table 2. These values are close

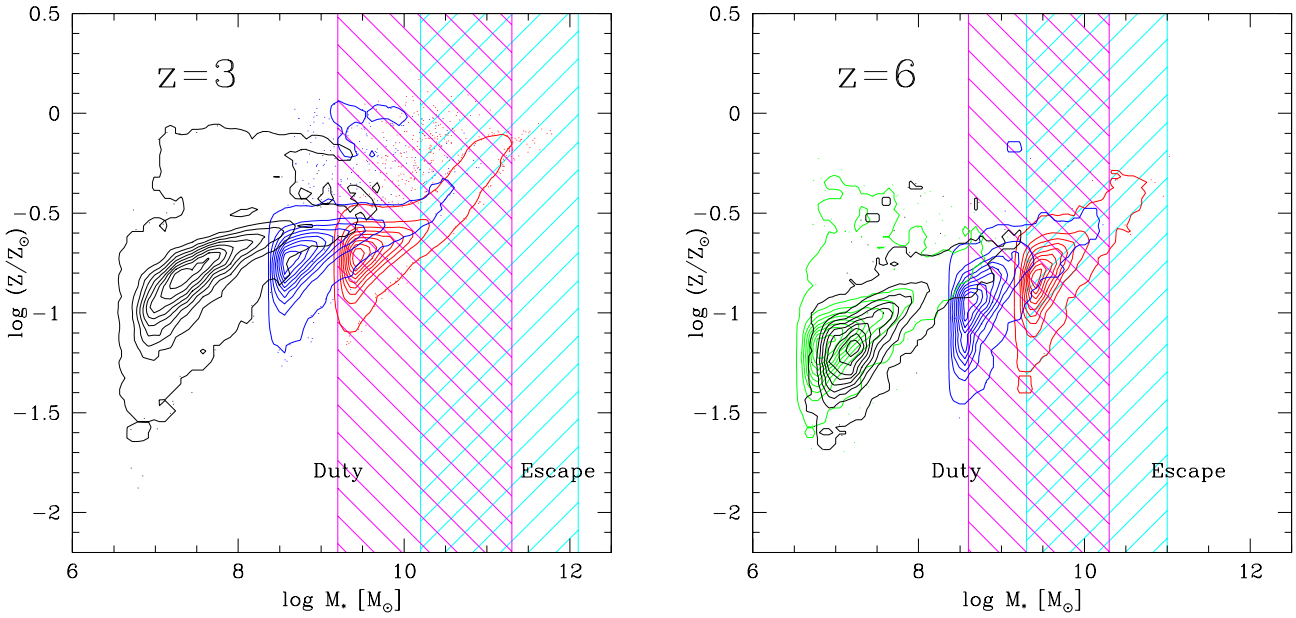

FIG. 6.— Galaxy stellar metallicity vs. galaxy stellar mass. The three sets of contours are for the Q5 (black), D5 (blue) and G6 (red) run from left to right. For $z = 6$, the result of the Q6 run is also shown with the green contour. The range of galaxy stellar mass for each scenario is indicated by the shade.

to the lower edge of the listed stellar mass ranges, because of the increasing number of low-mass galaxies in a cold dark matter universe. In this scenario, the LAEs with $\log L_{\rm Ly\alpha} = [42, 44]$ contribute only 18% (11%) of the total stellar mass density at $z = 3$ (6). This relatively low fraction owes to the steep faint-end slope of the stellar mass function (Fig. 3).

In the duty cycle scenario, currently observed LAEs correspond to slightly lower mass galaxies than in the escape fraction scenario:

$$\langle M_\star \rangle = 3.8 \times 10^9 \ (6.1 \times 10^8) \, M_\odot \text{ at } z = 3 \ (6) \qquad (10)$$

for the LAEs with $\log L_{\rm Ly\alpha} = [42, 44]$ in the D5 run. The fraction of stellar mass density contributed by the LAEs is higher in this scenario, amounting to 42% (29%) for $z = 3$ (6).

7. BLACK HOLES HOSTED BY LAES

The masses of black holes hosted by LAEs are also of significant interest, as they determine the AGN contribution to the total energy output from LAEs. We indicate the black hole masses in the top axes of Figure 5 assuming $M_\star/M_{\rm BH} \approx 0.004$ (0.005) at $z = 3$ (6), as suggested by the recent numerical simulations of galaxy mergers (Di Matteo et al. 2005; Robertson et al. 2006; Hopkins et al. 2007c) and observations (e.g. Peng et al. 2006). We find that the LAEs with $\log L_{\rm Ly\alpha} = [42, 44]$ host BHs with masses $\log M_{\rm BH} = [7.7, 9.7]$ ($z = 3$) and $[6.9, 8.7]$ ($z = 6$) for the escape fraction scenario, and $\log M_{\rm BH} = [6.7, 8.8]$ ($z = 3$) and $[6.3, 8.0]$ ($z = 6$) for the duty cycle scenario. If we instead assume the local value of $M_\star/M_{\rm BH} \approx 0.001$ (Kormendy & Gebhardt 2001), then the above mass ranges change to $\log M_{\rm BH} = [7.2, 9.2]$ ($z = 3$) and $[6.3, 8.1]$ ($z = 6$) for the escape fraction scenario, and $\log M_{\rm BH} = [6.2, 8.3]$ ($z = 3$) and $[5.7, 7.4]$ ($z = 6$) for the duty cycle scenario.

At $z = 3.1$, Ouchi et al. (2007) reported that the AGN fraction of LAEs is only $\sim 1\%$ for LAEs with $L_{\rm Ly\alpha} > 1 \times 10^{42} \, {\rm erg \, s^{-1}}$, but that the fraction is as high as 100% for the bright LAEs with $L_{\rm Ly\alpha} > 4 \times 10^{43} \, {\rm erg \, s^{-1}}$. On the other hand, they found no AGNs (nor LAEs) at $z = 5.7$ with a bright luminosity of $L_{\rm Ly\alpha} > 4 \times 10^{43} \, {\rm erg \, s^{-1}}$, and suggested that the number density of LAEs with AGN activities would drop from $z = 3$ to 6. Figure 5 shows that the mean BH mass for the LAEs with $\log L_{\rm Ly\alpha} = [42, 44]$ decreases from $z = 3$ to 6, which is at least consistent with the observed decrease of bright AGNs if BH mass is correlated with the strength of AGN activity.

8. LAE METALLICITY

In Figure 6, we show the galaxy stellar metallicity vs. stellar mass in our simulations. The metallicity of each galaxy is computed by summing up the metal mass in all constituent star particles, and then dividing by the total stellar mass of each galaxy. There is a weak positive correlation between the two quantities with significant scatter.

At $z = 6$, the majority of galaxies have $\log(Z/Z_\odot) < -0.5$, and the most massive ones with $\log M_\star > 10.5$ have $\log(Z/Z_\odot) > -0.5$. There are some outliers with $\log(Z/Z_\odot) > -0.5$ at the low-mass end of the distribution, which are small galaxies that have just started to undergo star formation and self-enrichment. Close to the resolution limit, the coarse sampling of the galactic winds leads to substantial numerical scatter in the metal loss, which in turn can temporarily produce high metallicities for some of the small galaxies. However, the fraction of such outliers is very small with $\sim 6\%$ (0.2%) of the total sample in the Q5 run at $z = 3$ (6).

At $z = 3$, the majority of galaxies still has $\log(Z/Z_\odot) < -0.5$, but the number of galaxies with $\log(Z/Z_\odot) > -0.5$ has increased significantly since $z = 6$, and the most massive ones with $\log M_\star > 11$ approach solar metallicity.

Since the galaxy stellar mass range is lower in the duty

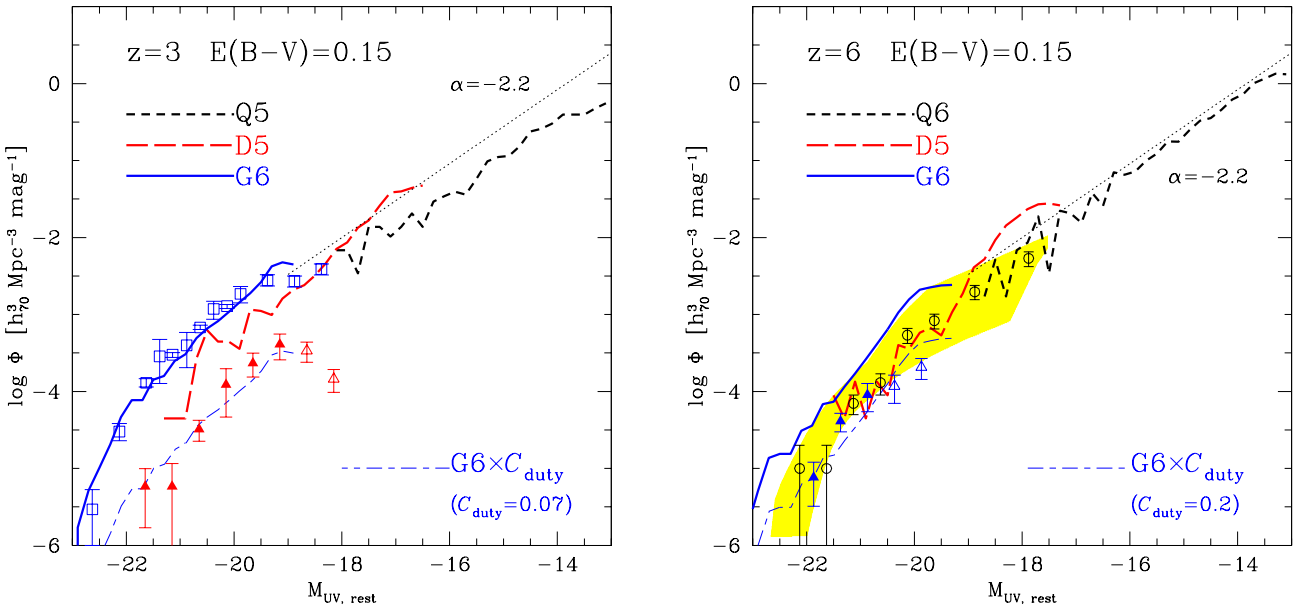

FIG. 7.— Rest-frame UV luminosity functions at $z = 3$ and $z = 6$. Thick lines are the original simulation results, and thin lines are those multiplied by $C_{\rm duty}$. The data points are $z = 3$ LBGs (Adelberger & Steidel 2000, blue open squares), UV LF of LAEs at $z = 3.1$ (Ouchi et al. 2007, red filled triangles), i-dropout LBGs at $z = 6$ (Bouwens et al. 2007, black open circles) and UV LF of LAEs at $z = 5.7$ (Ouchi et al. 2007, blue filled triangles). The two faintest data points of Ouchi et al. (2007) indicated with open triangles are less reliable owing to incompleteness. The yellow shade encompasses the current observational estimates by Bouwens et al. (2004); Bunker et al. (2004); Dickinson et al. (2004); Yan & Windhorst (2004); Malhotra et al. (2005); Beckwith et al. (2006). The black dotted line shows a power-law with a faint-end slope of $\alpha = -2.2$ in both panels with same normalization.

cycle scenario than in the escape fraction scenario, the corresponding galaxies have lower metallicity in general, as summarized in Table 2. Owing to the large scatter in the distribution, the difference in the metallicity range is not so large between the two scenarios, but the trend of lower metallicity in the duty cycle scenario is clearly seen in the mean metallicity values listed in Table 2. As expected, the mean metallicity at $z = 3$ is higher than at $z = 6$ by about a factor of 2 in both scenarios.

It would be useful to compare the mean metallicity of LAEs and LBGs. The mean metallicity of LBGs is known to be $\sim 1/3\, Z_\odot$ (e.g., Pettini 2004). At $z = 3$, the mean metallicity of LAEs in the escape fraction scenario is comparable to that of LBGs with $\langle Z/Z_\odot \rangle = 0.39$, while it is lower for the duty cycle scenario with $\langle Z/Z_\odot \rangle = 0.21$.

9. REST-FRAME UV LUMINOSITY FUNCTION

One of the interesting recent development in the observations of LAEs is that the rest-frame UV LF of LAEs is beginning to be constrained at the same time as the Lyα LF. This has been difficult in the past, because the UV continuum of LAEs tends to be faint, and large samples of LAEs were not available owing to limited sizes of the field-of-view (FoV) of the observations.

Figure 7 compares the simulated rest-frame UV LF with observational data. We adopt a uniform, moderate extinction of $E(B - V) = 0.15$ at both $z = 3$ and 6 following our previous work (Nagamine et al. 2004c; Night et al. 2006). This extinction value is the median value for the LBGs at $z \simeq 3$ (Shapley et al. 2001).

At $z = 3$, we obtain very good agreement between the G6 run (blue solid line) and the observed data of Adelberger & Steidel (2000, open squares) for LBGs. This agreement suggests that the SFR function (Fig. 2) of simulated galaxies at $z = 3$ is quite reasonable at least at the bright-end. We note that it is also reasonable that the D5 run underpredicts the observed data owing to its limited box size.

At $z = 6$, we show in Fig. 7 the data by Bouwens et al. (2007) for i-dropout LBGs. The yellow shade indicates the region covered by the Schechter function fits of other observational studies (Bouwens et al. 2004; Bunker et al. 2004; Dickinson et al. 2004; Yan & Windhorst 2004; Malhotra et al. 2005; Beckwith et al. 2006), which we estimated from Fig. 11 of Bouwens et al. (2007). The G6 run follows the upper envelope of the yellow shade and slightly overpredicts the data at $M_{UV} < -22$. Bouwens et al. (2006) reported that the extinction of $z = 6$ LBGs are lower than those of $z = 3$ ones, which would exacerbate the discrepancy between the simulation and observation at $z = 6$.

It is possible to improve the agreement between the G6 run and the observed data by increasing the assumed extinction for massive galaxies. For example, correlating the extinction with metallicity would boost the extinction in massive galaxies (Fig. 6), and make the bright-end of the LF steeper. However, here we choose not to resort to such an additional modeling, because this would cloud the interpretation of the comparison between simulation and observation.

Another possible cause for the overprediction of UV LF at the bright-end at $z = 6$ is that the current simulations lack the explicit implementation of AGN feedback. It is considered that the energy and momentum feedback from black holes suppress the star formation in massive galaxies at intermediate redshifts (e.g., Di Matteo et al. 2005; Springel et al. 2005; Hopkins et al. 2007b,a). The effects of AGN feedback on galaxy LFs at high redshifts can

be studied in the future using hydrodynamic simulations that treat AGN feedback explicitly (Di Matteo et al. 2007; Sijacki et al. 2007; Li et al. 2007).

10. EVOLUTION OF Lyα AND UV LF OF LAES

Currently there is no clear picture regarding the evolution of the observed rest-frame UV LF from $z = 6$ to 3. Some studies suggest a systematic brightening of the characteristic magnitude $M^*_{\rm UV,rest}$ by $0.5 - 1$ mag (Bouwens et al. 2006; Yoshida et al. 2006; Oesch et al. 2007; Bouwens et al. 2007). Other work argues for an evolution in the normalization ϕ^* (Beckwith et al. 2006) or in the faint-end slope (Yan & Windhorst 2004).

In our current simulations, there is not much evolution in the UV LF from $z = 6$ to 3, as already shown by Night et al. (2006), except that the $M^*_{\rm UV}$ becomes slightly brighter (see Fig. 13 of Bouwens et al. 2007, in which the comparison between simulations and observed data was performed explicitly) and α becoming slightly shallower, as can be seen in Fig. 7 when compared to the power-law slope of $\alpha = -2.2$ (dotted line). This trend is at least qualitatively consistent with the observed one by Bouwens et al. (2007). The galaxy stellar mass function evolves as shown in Fig. 3, but the evolution in the SFR (Fig. 2) cancels that out, resulting in little evolution in the UV LF.

Also shown in Fig. 7 are the UV LF *of LAEs* by Ouchi et al. (2007, filled triangles). Their data suggest that the number density of LAEs at $z = 3$ is only 10% that of LBGs', down to $M_{\rm UV} \simeq -20$ for the equivalent width (EW) limit of $40 - 60$ Å, whereas the LAE fraction at $z \sim 6$ increases to $50 - 100\%$ for the EW limit of $\simeq 30$ Å. Ouchi et al.'s LAE fraction at $z = 3$ is consistent with the earlier result by Shapley et al. (2003, $\sim 25\%$ with EW limit of 25 Å), but at $z \sim 6$, Ouchi et al.'s LAE fraction is higher than other spectroscopic studies of i'-dropout galaxies, which typically suggest $\sim 30\%$ (Dow-Hygelund et al. 2007; Stanway et al. 2004; Vanzella et al. 2006).

Let us first consider the duty cycle scenario. At $z = 3$, when we multiply the normalization of the simulated UV LF (which assumes uniform $E(B - V) = 0.15$) by $C_{\rm duty} = 0.07$ (i.e., LAE fraction of 7%), we obtain good agreement with the observed UV LF of LAEs. At $z = 6$, we again obtain a reasonable agreement with the observed UV LF of LAEs when we multiply the LBG UV LF by $C_{\rm duty} = 0.2$ (i.e., LAE fraction of 20%), as shown in the right panel of Fig. 7 with the short-dash long-dashed line. However, given that the LF of i'-dropout galaxies at $z \sim 6$ is still very uncertain and that our simulated LF might be overpredicting the UV LF at the bright-end, we cannot make a strong argument about the LAE fraction at this point. If current observations are underestimating the number of very bright i'-dropouts ($M_{\rm UV} \lesssim -22$) at $z = 6$ for some reasons (e.g., cosmic variance, limited FoV), then our simulations would be able to explain both the UV and Lyα LF of LAEs at $z = 3$ & 6 with LAE fractions of 7% & 20%, respectively, in the duty cycle scenario.

One problem in the above argument is that we implicitly assumed that the UV extinction of LAEs is also $E(B - V) = 0.15$. However, recent observations (Ouchi et al. 2007; Gronwall et al. 2007) suggest much lower extinction for LAEs with $E(B - V) < 0.05$. If this is the case, then the duty cycle scenario would not be able to explain the UV and Lyα LF of LAEs self-consistently with above values of $C_{\rm duty}$. Furthermore, the escape fraction scenario completely fails to explain the UV LF of LAEs if the extinction of LAEs is systematically lower than that of LBGs. Because this scenario assumes that "*all* LBGs emit Lyα emission following Eq. (2) that are then attenuated uniformly by a factor of $f_{\rm Ly\alpha}$", the escape fraction scenario would predict a *brighter* UV LF for LAEs than that of LBGs, which is contradictory to the observed data.

At this point there is no easy way out, unless we start considering the possibility that the LAEs are a separate population from LBGs. It is certainly possible that the majority of LAEs are low-mass galaxies with low extinction and low metallicity. This is also consistent with what we have argued for in Fig. 5 for the duty cycle scenario. Even if we bring a fraction of low-mass galaxies in the UV LF with $E(B - V) = 0.0$ and multiply it by a certain value of $C_{\rm duty}$, the slope of the LAE UV LF does not agree with the data. This suggests variable extinction for LAEs, and we could model this by correlating extinction with metallicity (e.g., Finlator et al. 2006), although we discuss the problems in this approach in § 13. Since the purpose of our paper is *not* to introduce models more complicated than the simulation itself, we choose not to pursue any additional modeling.

11. CORRELATION FUNCTION AND BIAS OF LAES

The correlation function of LAEs provides interesting constraints on the distribution of LAEs, and it might help to discern the two scenarios that we have discussed above. We compute the auto-correlation function (CF) of LAEs using the Landy & Szalay (1993) estimator, $(DD-2DR+RR)/RR$, and show the results in Figure 8. Since the current luminosity limit of the observed LAEs is $\log L_{\rm Ly\alpha} \approx 42.0$ for the $z = 3$ sample, we restricted our sample to those with $\log L_{\rm Ly\alpha} > 42.0$ for both $z = 3$ & 6 to measure the correlation function. At $z = 6$, the current luminosity limit is higher at $\log L_{\rm Ly\alpha} > 42.5$ because of the greater distances to the sources, but we kept the luminosity limit the same for our calculations to obtain a reasonably strong correlation signal with a sufficient number of simulated galaxies.

In the escape fraction scenario (Fig. 8a), the observed luminosity range is completely covered by the G6 run, so it is well-suited for this calculation. Using the data points in the range of $\log r = [0.0, 1.3]$, we perform a least square fit to the power-law function $\xi(r) = (r_0/r)^\gamma$, and find $(r_0[h^{-1}\,{\rm Mpc}], \gamma) = (5.5, 1.67)$ and $(4.4, 1.68)$ for $z = 3$ & 6, respectively. The CF at $z = 3$ has a longer correlation length than at $z = 6$, because the mean stellar mass of LAEs at $z = 3$ is higher (§ 6). The slopes of the CF at the two epochs are very close to each other with $\gamma \approx 1.7$. Our values of (r_0, γ) are similar to those of LBGs at $z \approx 3 - 6$ (Ouchi et al. 2004b; Adelberger et al. 2005), which makes sense because the mean stellar mass of LAEs in the escape fraction scenario is comparable to that of LBGs with a few times $10^{10}\,M_\odot$ at $z = 3$.

For the duty cycle scenario, the observed data points of Ouchi et al. (2007) are fully covered only by the D5 run (see Fig. 4). The resolution limit of the G6 run corresponds to $\log L_{\rm Ly\alpha} \approx 43$ in this scenario, therefore we cannot use the G6 run to measure the CF for the

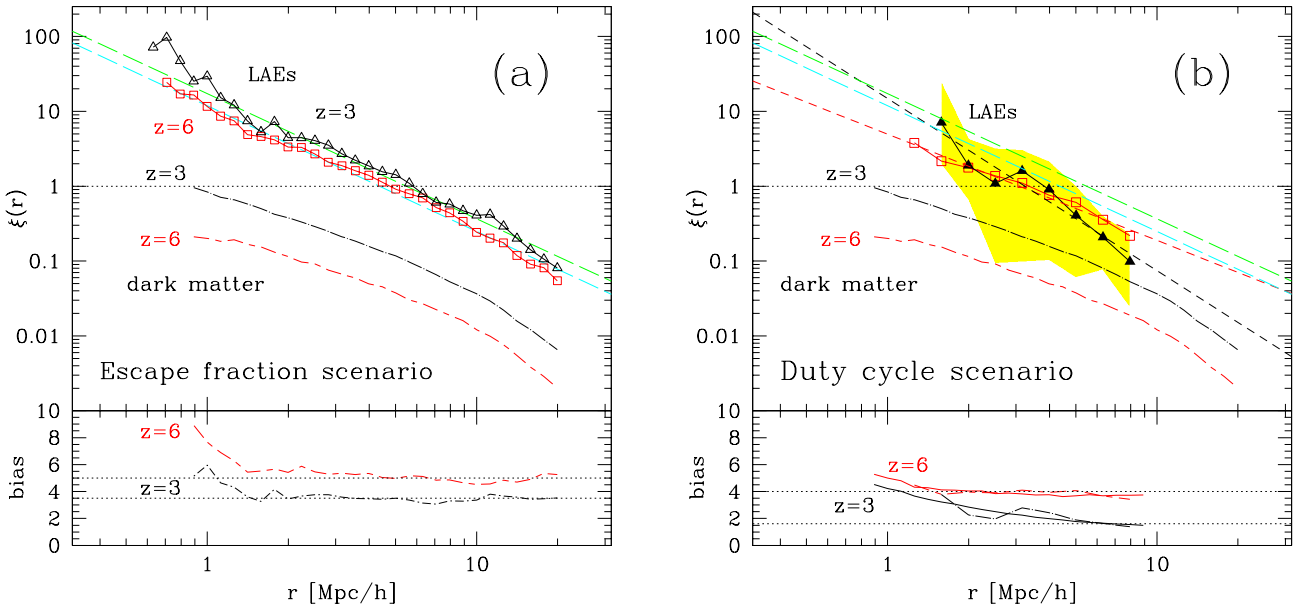

FIG. 8.— Auto-correlation function of LAEs at $z = 3$ & 6. The G6 run was used for the escape fraction scenario (panel [*a*]), and the D5 run was used for the duty cycle scenario (panel [*b*]). The two *long-dashed* lines are the least square fits to the data points for the escape fraction scenario. The parameters of the power-law fits are listed in Table 2. In the duty cycle scenario, the sample size is small (101 & 406 LAEs at $z = 3$ & 6), therefore we used 20 different data sets to examine the variance of the CF (shown by the yellow shade for $z = 3$). The mean of the 20 trials is shown by the data points, and the power-law fits to the mean are shown in *short-dashed* lines. The variance at $z = 6$ is smaller than at $z = 3$ owing to larger sample. The bottom panels show the bias of LAEs against dark matter. For the duty cycle scenario, the bias was computed for both using the direct simulation result (*short-long-dash* and *dot-dashed* lines) and using the power-law fits (solid lines).

duty cycle scenario with the same luminosity limit of $\log L_{\mathrm{Ly}\alpha} = 42.0$. As discussed in § 5.2, the number density of sources in the simulation has to be reduced by a factor of $C_{\mathrm{duty}} = 0.07$ (0.2) at $z = 3$ (6) in this scenario. In the D5 run, there are $N_{>42} = 1439$ (2032) sources with $\log L_{\mathrm{Ly}\alpha} \geq 42.0$ at $z = 3$ (6), therefore we need to select only $N_{>42} \times C_{\mathrm{duty}} = 101$ (406) LAEs in the comoving volume of $(33.75\,h^{-1}\,\mathrm{Mpc})^3$. Owing to the small sample size, the CF signal for the duty cycle scenario is somewhat noisy. We therefore randomly resample 20 different data sets with above LAE numbers, and calculate the mean of the 20 different trials to reduce the noise. We find that the CFs drop off at $r > 8\,h^{-1}\,\mathrm{Mpc}$ owing to limited box size, therefore we only use data at $r < 8\,h^{-1}\,\mathrm{Mpc}$ for the power-law fit. Fig. 8b shows that the CF at $z = 3$ is steeper with $\gamma = 2.3$, although we consider that this result is not reliable owing to small sample size (101 LAEs). At $z = 6$, we obtain a shallower slope of $\gamma = 1.49$ and $r_0 = 3.1\,h^{-1}\,\mathrm{Mpc}$. In fact, if we increase the sample size at $z = 3$ to the same size as that at $z = 6$ (406 LAEs, corresponding to $C_{\mathrm{duty}} = 0.28$, which will overpredict the Lyα LF), then we obtain a similar signal to that at $z = 6$ with $\gamma = 1.61$ and $r_0 = 3.9\,h^{-1}\,\mathrm{Mpc}$. Therefore we consider that the steep slope of $z = 3$ result is simply owing to the limited sample size.

The correlation length is smaller in the duty cycle scenario than in the escape fraction scenario with $r_0 \simeq 3\,h^{-1}\,\mathrm{Mpc}$, which is reasonable given the lower mean stellar mass of LAEs in this scenario. The sparse sampling also prohibits us from obtaining the CF signal at $r \lesssim 1.5\,h^{-1}\,\mathrm{Mpc}$ in the duty cycle scenario. In order to measure the CF for the duty cycle scenario more reliably, we need a simulation box size of $L_{\mathrm{box}} \gtrsim 100 h^{-1}\,\mathrm{Mpc}$ with a resolution comparable to that of the D5 run. This should become possible in the near future thanks to rapidly increasing computing resources.

11.1. *Bias of LAEs*

The lower panels of Fig. 8 show the bias relative to the clustering of the mass, which is defined as $b \equiv \sqrt{\xi_{\mathrm{gal}}/\xi_{\mathrm{dm}}}$. We compute the correlation function of dark matter by randomly sampling 200,000 dark matter particles in the G6 run. Using the D5 run yields very similar results on scales of $r = 1 - 8\,h^{-1}\,\mathrm{Mpc}$. In both scenarios, the bias is a slowly decreasing function with increasing distance. Even though the value of r_0 is greater at $z = 3$, the bias relative to the dark matter is greater at $z = 6$, because the growth in dark matter structure significantly increases the normalization of the dark matter CF from $z = 6$ to 3.

In the escape fraction scenario (Fig. 8a), we find $b \simeq 3.5$ (5.0) at $r = 1.5 - 10\,h^{-1}\,\mathrm{Mpc}$ for $z = 3$ (6), crossing the above value at $r = 4 - 5\,h^{-1}\,\mathrm{Mpc}$. At smaller scales ($r \lesssim 1.5\,h^{-1}\,\mathrm{Mpc}$), the bias increases up to $b \sim 6$ (9) at $z = 3$ (6). This could owe to the excess clustering of galaxies on small scales as discovered by Ouchi et al. (2005a), although Ouchi's data at $z = 4.0$ suggest that this increase in bias occurs at $r \lesssim 0.2\,h^{-1}\,\mathrm{Mpc}$. The increase of clustering on small-scales can be ascribed to the substructures within each halo ("one-halo" term). It is possible that the simulation is still lacking some physics or resolution to capture the correct scale for this transition. On large scales, the correlation function of dark matter seems to turn down, and at $z = 6$ the bias somewhat increases at $r \gtrsim 15\,h^{-1}\,\mathrm{Mpc}$, which is probably a box-size effect.

In the duty cycle scenario (Fig. 8b), we use both the power-law fits and the actual simulation results to compute the bias. The calculation using the power-law yields monotonically declining functions with increasing distance. At $z = 3$ the bias decreases from 4.5 to 1.5, and at $z = 6$ from 5.3 to 3.7 with increasing distance. The calculation using the direct simulation CF shows more noisy behavior, wiggling around the power-law result. At $z = 3$ the bias decreases from 3.8 to 1.4 at $r = 1.6-8\,h^{-1}$ Mpc. At $z = 6$, the wiggle is smaller and the *long-short-dashed* line agrees well with the power-law result, yielding $b \simeq 4$ at $r = 1.5-7\,h^{-1}$ Mpc, which is contrasted with $b \simeq 5$ in the escape fraction scenario.

The comparison to some of the observational estimates yields somewhat mixed results, but in general support the duty cycle scenario. Kovač et al. (2007) found $r_0 = 4.61 \pm 0.6\,h^{-1}$ Mpc (taking the contamination by randomly distributed objects into account) and $b \sim 3.7$ for the LAEs at $z \sim 4.5$ in the LALA survey (Rhoads et al. 2000). Ouchi et al. (2003) found $r_0 = 3.5 \pm 0.3\,h^{-1}$ Mpc for $z = 4.86$ LAEs. Kovač et al. (2007) pointed out that Ouchi's maximum permitted value would be $r_0 = 4.5 \pm 0.4\,h^{-1}$ Mpc when the 20% contamination by low-z galaxies (Shimasaku et al. 2004) is taken into account. Our results for the escape fraction scenario at $z = 3$ & 6 nicely bracket Kovač et al.'s results at $z \simeq 4.5$. The bias values in the duty cycle scenario brackets the Kovač et al.'s result, but the value of r_0 is lower than theirs or at the lower edge of Ouchi et al.'s estimate.

Gawiser et al. (2007) reported $r_0 = 3.6^{+0.8}_{-1.0}$ Mpc and $b = 1.7^{+0.3}_{-0.4}$ for LAEs at $z = 3.1$. Our CF results at $z = 3$ for the duty cycle scenario are in good agreement with Gawiser et al.'s estimates. This is consistent with the nice agreement between our simulations and the observed data seen in Fig. 5 for the duty cycle scenario at $z = 3$. Our results from the escape fraction scenario at $z = 3$ do not agree with Gawiser et al.'s data. At $z = 6$, our result of $b = 3.7$ at $r \sim 8h^{-1}$ Mpc in the duty cycle scenario agrees well with $b = 3.4 \pm 1.8$ derived by Ouchi et al. (2005b) for LAEs at $z \sim 5.7$. These comparisons again support the duty cycle scenario.

12. COSMIC VARIANCE

It is clearly difficult to conduct a deep, wide-field survey of high-z galaxies and obtain a statistically representative sample of galaxies in a large volume of space. If the survey area is too small, then the observed sample may not be representative of the total population owing to the large-scale structure of the Universe, and the estimated LF would scatter around the true LF. This is one manifestation of the so-called "cosmic variance".

In order to estimate the cosmic variance in our results, we use eight sub-volumes of $(45 \times 45 \times 44\,h^{-1}\,\mathrm{Mpc})^3$ in the G6 run and derive the LF from each sub-volume (Figure 9). For our adopted flat Λ cosmology, a viewing angle of 1 degree corresponds to about comoving $100\,h^{-1}$ Mpc at $z = 6$, so the above subvolume corresponds to a field with FoV $= (0.45\ \mathrm{deg})^2 \approx 0.2\ \mathrm{deg}^2$. The thickness of $44\,h^{-1}$ Mpc was chosen to match the data of Ouchi et al. (2007, Fig. 18), but the exact value is not so important, as we would obtain a similar result even if we adopted $(50\,h^{-1}\,\mathrm{Mpc})^3$ subvolumes. Here we used $f_{\mathrm{Ly}\alpha} = 0.15$ as we did in Fig. 4.

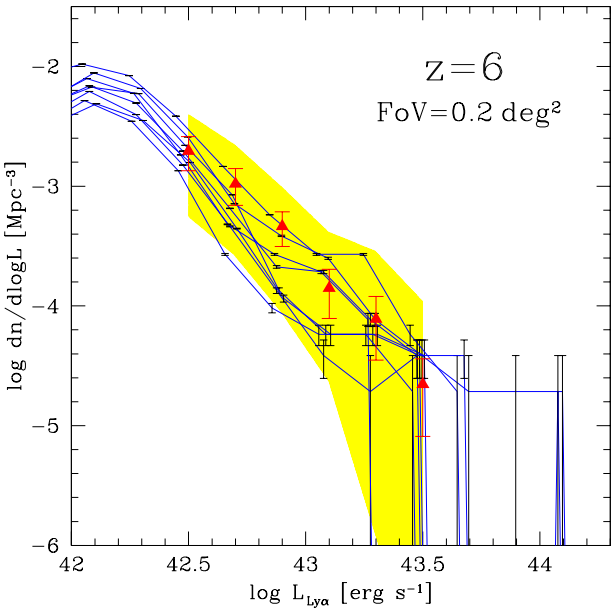

FIG. 9.— Lyα luminosity function at $z = 6$ measured in the eight subvolumes of $(45\times45\times44\,h^{-1}\,\mathrm{Mpc})^3$ in the G6 run, corresponding to a 0.2 deg^2 field of view. The error bars show Poisson errors in each subvolume, slightly offset from each other to avoid overlap. The red filled triangle data points are from Ouchi et al. (2007), and the yellow shade shows the variance of their five 0.2 deg^2 fields.

The large scatter of LFs seen in Fig. 9 owes to cosmic variance, and it clearly exceeds Poisson errors shown by the error bars. The red filled triangle is the data by Ouchi et al. (2007) and the yellow shade is the variance of their data from five 0.2 deg^2 fields. The cosmic variance we find is consistent with the field-to-field variation observed by Ouchi et al. (2007, Fig. 18), as well as the data of Shimasaku et al. (2004) that shows very different distribution of LAEs at $z = 4.79$ and 4.86, separated by $\sim 40\,h^{-1}$ Mpc in the same FoV (see also Hu & Cowie 2006). At $\log L_{\mathrm{Ly}\alpha} = 43.0$, the cosmic variance in the vertical direction is almost an order of magnitude in $\mathrm{d}n/\mathrm{d}\log L_{\mathrm{Ly}\alpha}$, and ~ 0.6 dex in the horizontal direction (i.e., $\log L_{\mathrm{Ly}\alpha}$). At $\log L_{\mathrm{Ly}\alpha} > 43.5$, the Poisson error bar is large, because one object in the above subvolume corresponds to the data point of $\mathrm{d}n/\mathrm{d}\log L_{\mathrm{Ly}\alpha} = -4.72^{+0.30}_{-\infty}$. Our result shows that a survey field of $\gtrsim 1$ deg^2 is necessary to obtain a reliable estimate of Lyα & UV LFs at $z = 6$.

13. CONCLUSIONS & DISCUSSIONS

Encouraged by the earlier successes in describing the properties of LBGs at $z = 3-6$ using cosmological SPH simulations (Nagamine et al. 2004c; Night et al. 2006), we considered two simple scenarios to explain the luminosity functions of LAEs at $z = 3$ and 6. These scenarios are very simple, but should capture the two extreme cases of LAE properties. The true physical nature of LAEs could be a combination of the two scenarios. We summarize the parameters associated with the two scenarios in Table 2. The main conclusions of our work can be summarized as follows:

- In our simulations, star formation becomes progressively less efficient from $z = 6$ to 3, especially for

the massive galaxies with $M_\star > 10^{10}\,M_\odot$. This evolution in the SF efficiency largely compensates the growth in the galaxy mass function, yielding little evolution in the rest-frame UV LF. We provide a fitting formula for the SFR–$M_\star$ relationship in Eq. (1). The SFR function (Fig. 2) does not evolve very much from $z = 6$ to 3.

- We investigate two simple scenarios to characterize the properties of LAEs: the "*escape fraction*" scenario and the "*duty cycle*" scenario. By matching the simulated Lyα LF of LAEs to the observed one by Ouchi et al. (2007), we find that the *effective* escape fraction of Lyα photons is $f_{\rm Ly\alpha} = 0.1$ (0.15) for $z = 3$ (6), where the effect of IGM attenuation is included. In the case of the duty cycle scenario, we find that the duty cycle parameter is $C_{\rm duty} = 0.07$ (0.2) for $z = 3$ (6), after correcting the observed LF for the IGM attenuation effect. If we do not correct for IGM attenuation, we obtain $C_{\rm duty} = 0.06$ for both $z = 3$ and 6.

- In both scenarios, we find that $f_{\rm dust} \approx 0.1$ at $z = 3$ and $f_{\rm dust} \approx 0.2 - 0.4$ at $z = 6$. In detail, if we correct for the IGM attenuation effect with $f_{\rm IGM} = 0.82$ (0.52) and assume $f_{\rm esc}^{\rm ion} = 0.06$ (0.2) at $z = 3$ (6), then we obtain $f_{\rm dust} = 0.13$ (0.36) at $z = 3$ (6), respectively. If we instead adopt $f_{\rm IGM} = 1.0$ and the same values of $f_{\rm esc}^{\rm ion}$, then we find $f_{\rm dust} = 0.11$ (0.19) for $z = 3$ (6).

- The mean stellar mass of LAEs is lower in the duty cycle scenario than in the escape fraction scenario, as summarized in Table 2. This implies lower mean values of BH mass, SFR and metallicity, as well as a lower amplitude of the correlation function in the duty cycle scenario. The mean stellar mass of LAEs is higher at $z = 3$ than at $z = 6$, as expected in the hierarchical structure formation model.

- In the escape fraction scenario, the auto-correlation function of LAEs is similar to that of LBGs with $r_0 = 4 - 6\,h^{-1}\,$Mpc and $\gamma \simeq 1.7$ for both $z = 3$ and 6. The corresponding galaxy–dark matter bias is $b \simeq 3.5$ (5.0) at $r = 1.5 - 10\,h^{-1}\,$Mpc for $z = 3$ (6). These results bracket the observational estimates by Kovač et al. (2007) at $z \sim 4.5$. On the other hand, the CF in the duty cycle scenario has a shorter correlation length of $r_0 \simeq 3\,h^{-1}\,$Mpc and the bias of $b = 1.6 - 4.6$ ($z = 3$) & 4 ($z = 6$), in good agreement with the observational estimates by Gawiser et al. (2007) at $z \sim 3$. In both scenarios, the bias parameter decreases with increasing distance.

- We find that the effect of cosmic variance on LF estimates can be quite strong. The Lyα LFs at $z = 6$ measured in 8 different fields of ~ 0.2 deg^2 have a variance of $\sim 1.0\,$dex in $\mathrm{d}n/\mathrm{d}\log L_{\rm Ly\alpha}$ at $\log L_{\rm Ly\alpha} = 43.0$, and $\sim 0.6\,$dex in the horizontal direction (i.e., $\log L_{\rm Ly\alpha}$). This result suggests that a survey field of $\gtrsim (1\ \mathrm{deg})^2$ is necessary to measure the Lyα and UV LFs at $z = 6$ reliably.

- We find that the duty cycle scenario is preferred over the escape fraction scenario through the comparisons with various observational data, including $M_\star$, SFR, Lyα & UV LFs, correlation functions, and bias relative to the dark matter distribution. In particular, the duty cycle scenario succeeds in explaining the the rest-frame UV LFs of *both* LBGs and LAEs at $z = 3$ & 6, provided $E(B-V) \approx 0.15$ for both population. However, if the extinction of UV photons in LAEs is systematically lower than that of LBGs with $E(B-V) < 0.05$ as the recent observations suggest (Ouchi et al. 2007; Gronwall et al. 2007), then our simple models (with *uniform* $f_{\rm Ly\alpha}$ or $C_{\rm duty}$) fail to explain the UV LFs of LAEs and LBGs simultaneously. In this case, the escape fraction scenario completely breaks down, because it would predict a brighter UV LF of LAEs at $z = 3$, contrary to the observation.

In the case of duty cycle scenario, additional modeling would be necessary to accommodate lower extinction for LAEs, such as variable extinction and treating LBGs and LAEs as separate populations. The assumption of linear SFR – $L_{\rm Ly\alpha}$ relationship (Eq. 2) and uniform $f_{\rm dust}$ & $E(B-V)$ imply that galaxies with high SFR would appear as bright LBGs with high $L_{\rm Ly\alpha}$. If we further assume that $E(B-V)$ is positively correlated with metallicity as in Finlator et al. (2006), then the mass-metallicity relationship implies that the bright LBGs would be relatively massive galaxies with high extinction. Combined, this means that high $L_{\rm Ly\alpha}$ sources have high extinction, which is the opposite of what is found observationally (Shapley et al. 2003; Ouchi et al. 2007; Gronwall et al. 2007; Gawiser et al. 2007). Therefore, to assign lower extinction for LAEs, one must invoke some other physical processes, such as galactic outflows, that could temporarily reverse the above relationship between $L_{\rm Ly\alpha}$ and $E(B-V)$.

If the duty cycle scenario is really the correct one, then it could explain both Lyα and UV LFs of LAEs as follows: in the universe as early as $z = 6$, LBGs are actively forming stars, and as much as 20% ($C_{\rm duty} = 0.2$) of them would appear as LAEs (right panel of Fig. 7). If our simulations overpredict the UV LF of LBGs at $z = 6$, then this fraction could increase even further. By the time the universe has evolved to $z = 3$, star formation becomes less efficient owing to the lower mean density and less supply of infalling gas than at $z = 6$. The extinction of Lyα photons by dust also becomes stronger at $z = 3$ ($f_{\rm dust} \sim 0.1$). Only a small fraction ($C_{\rm duty} = 0.07$) of LBGs now appear as LAEs. Our values of $C_{\rm duty}$ nicely bracket the result obtained by Malhotra & Rhoads (2002, $C_{\rm duty} = 0.075 - 0.15$ at $z = 4.5$). If the star formation time-scale for the $z = 3$ LBGs is $\sim 200\,$Myr, then the life-time of LAEs at $z = 3$ would be $\sim 14\,$Myr according to the above duty cycle parameter. Ages between several Myr to 100 Myr are supported by recent observations (Gawiser et al. 2006; Lai et al. 2007a,b; Pirzkal et al. 2007). We remark that sporadic star formation histories are automatically included in our results, since they occur generically in our dynamic simulations (see Nagamine et al. 2005). Therefore, the values of $C_{\rm duty}$ in this paper characterize the

duty cycle *on top of* the intermittency of the SF activity.

Because we adopted a single relationship between SFR and Lyα luminosity (Eq. 2), we are essentially assuming that the equivalent width (EW) distribution of the Lyα emission line is a δ-function at ~ 70 Å.[6] This is obviously oversimplified, given that the actually observed data has a fairly wide distribution (e.g., Fig. 23 of Ouchi et al. 2007). One can easily accommodate a model that assumes a certain distribution of EW by, e.g., linking it to the scatter in the dust and metallicity distribution, and observe its effect on the LF. Kobayashi et al. (2007) performed such an exercise using a semi-analytic model of galaxy formation, and showed that the bright-end of the Lyα LF can be described better with such a treatment. Currently it is not clear whether our simulation is overpredicting the Lyα LF at the bright-end, because there are no reliable data at $\log L_{\rm Ly\alpha} > 43.5$ (see Fig. 4). If future observations show that there is a sharp exponential cutoff at $\log L_{\rm Ly\alpha} > 43.5$, we would be able to make stronger arguments on the possible connections between feedback effects and the bright-end of the Lyα LF. We note that our current simulations already include the effect of SN feedback and galactic outflows as described in § 2. Given these uncertainties, we decided not to invoke an additional model for the EW distribution on top of what has been modeled in the simulation.

Davé et al. (2006) computed the Lyα LF using cosmological SPH simulation in a similar fashion to our present work. They assumed Lyα emission of $2.44 \times 10^{42}\,{\rm erg\,s^{-1}}$ per SFR $[M_\odot\,{\rm yr^{-1}}]$ (Schaerer 2003) and took the metallicity variation into account. They argued that they obtain good agreement with the data of Santos et al. (2004) at $\log L_{\rm Ly\alpha} = [40.5, 42.5]$ if they assume $f_{\rm Ly\alpha} = 0.02$. However, the LF data points of Santos et al. (2004) are based on only a few objects and their normalization seems to be too low to smoothly connect with the data points of Ouchi et al. (2007) at $\log L_{\rm Ly\alpha} > 42$, as shown by the yellow shade in Fig. 4. Our simulations suggest that the LF at $L_{\rm Ly\alpha} = [40.5, 42.5]$ would be higher by a factor of ~ 5 than that of Santos et al. (2004) when we match our results to the data of Ouchi et al. (2007). We also point out that, according to what we discussed in § 12, the simulation box size used by Davé et al. (2006) (comoving $33h^{-1}$ Mpc) was too small to obtain a reliable LF at the bright-end. Had they used a simulation with a larger box size and matched their results to the data by Ouchi et al. (2007), we expect that they would have obtained a value of $f_{\rm Ly\alpha}$ similar to ours. Their galaxy correlation function at $z = 6$ is also lower than ours, probably owing to the same reason of a small box size. We note, however, that the galaxy stellar mass function (in the mass range that they simulated) and the bias in the two work are consistent with each other.

The value of $f_{\rm Ly\alpha} = 0.02$ assumed by both Davé et al. (2006) and Le Delliou et al. (2006) is significantly smaller than our value of $f_{\rm Ly\alpha} \simeq 0.1$. It is not easy to understand the source of this difference unless we compare the SFR function (Fig. 2) and the effect of dust attenuation in each model in detail. At least in the case of Davé et al. (2006), they may have underestimated the value of $f_{\rm Ly\alpha}$ by adjusting the results from a small simulation box size to the data of Santos et al. (2004). On the other hand, Kobayashi et al. (2007) argued for a much larger value for the escape fraction, $f_{\rm esc} \sim 0.8$, by incorporating the effects of outflows from starburst galaxies. As we described earlier, our simple escape fraction model fails to reproduce the UV LF of LAEs if their extinction is systematically lower than that of LBGs. It would be interesting to see what the above semi-analytic models predict on the joint constraint of the UV LF of LAEs and LBGs at $z = 3 - 6$.

Another source of uncertainty in the present work is the IMF. It is possible that the IMF changes as a function of redshift, metallicity, and environment (e.g., Larson 1998). Recently there have been several suggestions that some of the observational data can be better explained if the IMF becomes "top-heavy" or "bottom-light" towards high-z (e.g., Baugh et al. 2005; Chary 2007; van Dokkum 2007). It would also mitigate the apparent discrepancy between the data on extinction corrected SFR density and stellar mass density (e.g., Nagamine et al. 2004a; Nagamine et al. 2006a; Fardal et al. 2007; Davé 2007; Wilkins et al. 2008). If indeed the IMF is top-heavy at high-z, then the conversion factor in Eq. (2) could increase by a factor of ~ 2 (Schaerer 2003), and our intrinsic Lyα LF would be brighter by the same factor. In this case, the values of $f_{\rm Ly\alpha}$ and $C_{\rm duty}$ should be decreased by similar factors. The top-heavy IMF would also disrupt the agreement of the UV LF of LBGs at $z = 3$ between simulations and the observed data, and exacerbate the discrepancy between the simulation and the observed data at $z = 6$. As far as the Lyα & UV LFs of LAEs are concerned, we do not see any strong reasons to invoke a top-heavy IMF based on our comparisons, although we cannot rule out the possibility of top-heavy IMF given various uncertainties discussed in this paper.

ACKNOWLEDGMENTS

KN is grateful to Steve Furlanetto, Eric Gawiser and Kazuhiro Shimasaku for useful discussions on the properties of LAEs. The simulations and analyses for this paper were performed at the Institute of Theory and Computation at Harvard-Smithsonian Center for Astrophysics and UNLV Cosmology Computing Cluster.

[6] We calculated the EW as follows: EW $= L_{\rm Ly\alpha}/L_\lambda(1216\mathring{A}) = L_{\rm Ly\alpha}/([c/\lambda^2]L_\nu[1216\mathring{A}]) = 70\,\mathring{A}$, where we used $L_{\rm Ly\alpha} = 10^{42}\,{\rm erg\,s^{-1}}$ per SFR from Eq. (2), and $L_\nu(1216\mathring{A}) = L_\nu(1500\mathring{A}) = 7 \times 10^{27}\,{\rm erg\,s^{-1}\,Hz^{-1}}$ per SFR for a Salpeter IMF with mass limits $[0.1, 100]M_\odot$ (Madau et al. 1998; Kennicutt 1998) assuming that the continuum spectrum of starburst galaxies is flat at UV wavelengths.

REFERENCES

Adelberger, K. L. & Steidel, C. C. 2000, ApJ, 544, 218
Adelberger, K. L., Steidel, C. C., Pettini, M., Shapley, A. E., Reddy, N. A., & Erb, D. K. 2005, ApJ, 619, 697
Adelberger, K. L., Steidel, C. C., Shapley, A. E., & Pettini, M. 2003, ApJ, 584, 45
Barton, E. J., Davé, R., Smith, J.-D. T., Papovich, C., Hernquist, L., & Springel, V. 2004, ApJ, 605, L1

TABLE 2
Summary of Two Scenarios

Parameter	Escape Fraction Scenario $z = 3$	Escape Fraction Scenario $z = 6$	Duty Cycle Scenario $z = 3$	Duty Cycle Scenario $z = 6$
$f_{\rm Ly\alpha}$ [a]	0.10	0.15	—	—
$f_{\rm IGM}$ [b]	0.82 (1.0)	0.52 (1.0)	0.82 (1.0)	0.52 (1.0)
$f_{\rm esc}^{\rm ion}$ [c]	0.06	0.20	—	—
$f_{\rm dust}$ [d]	0.13 (0.11)	0.36 (0.19)	—	—
$C_{\rm duty}$ [e]	—	—	0.07 (0.06)	0.2 (0.06)
$\log(M_\star/M_\odot)$ [f]	$[10.2, 12.1]$	$[9.3, 11.0]$	$[9.2, 11.3]$	$[8.6, 10.3]$
$\langle M_\star/M_\odot \rangle$ [g]	2.5×10^{10}	1.9×10^9	3.8×10^9	6.1×10^8
$\rho_\star$ fraction [h]	0.18	0.11	0.42	0.29
$\log(M_{\rm BH}/M_\odot)$ [i]	$[7.7, 9.7]$	$[6.9, 8.7]$	$[6.7, 8.8]$	$[6.3, 8.0]$
$\langle M_{\rm BH}/M_\odot \rangle$ [j]	1.0×10^8	9.5×10^6	1.5×10^7	3.1×10^6
$\log(Z/Z_\odot)$ [k]	$[-0.7, 0.1]$	$[-1.3, -0.3]$	$[-1.0, 0.1]$	$[-1.4, -0.5]$
$\langle Z/Z_\odot \rangle$ [m]	0.39	0.17	0.21	0.11
r_0 [n]	5.5	4.4	(3.2)	3.1
γ [p]	1.67	1.68	(2.30)	1.49
b [q]	3.5 (< 6.0)	5.0 (< 8.9)	(1.6–4.6)	4.0

Note. — Summary of various parameter values in the two scenarios discussed in this paper.
a: *Effective* escape fraction of Lyα photons including the effect of IGM attenuation (§ 5.1).
b: IGM attenuation factor computed by following Madau (1995) prescription (§ 5.1). The case for $f_{\rm IGM} = 1.0$ is given in parenthesis.
c: Escape fraction of ionizing photons taken from Inoue et al. (2006, Fig. 3) (§ 5.1).
d: Extinction of Lyα photons by the local dust (§ 5.1). The case for $f_{\rm IGM} = 1.0$ is given in parenthesis.
e: Duty cycle (or fractional life time) of LAEs after correcting for the IGM attenuation effect (§ 5.2). The case for $f_{\rm IGM} = 1.0$ is given in parenthesis.
f: Stellar mass range of LAEs with $\log L_{\rm Ly\alpha} = 42 - 44$ (§ 6).
g: Mean stellar mass of LAEs with $\log L_{\rm Ly\alpha} = 42 - 44$ (§ 6).
h: Fraction of stellar mass density contained in LAEs with $\log L_{\rm Ly\alpha} = 42 - 44$ (§ 6).
i: Mass range of black holes hosted by LAEs with $\log L_{\rm Ly\alpha} = 42 - 44$ (§ 7).
j: Mean mass of BHs hosted by LAEs with $\log L_{\rm Ly\alpha} = 42 - 44$ (§ 7).
k: Stellar metallicity range LAEs with $\log L_{\rm Ly\alpha} = 42 - 44$ (§ 8).
m: Mean stellar metallicity of LAEs with $\log L_{\rm Ly\alpha} = 42 - 44$ (§ 8).
n: Correlation length of LAEs (§ 11).
p: Slope of the auto-correlation function of LAEs (§ 11).
q: Bias parameter of LAEs against dark matter distribution. For the escape fraction scenario, the maximum values at $r \simeq 0.9\,h^{-1}$ Mpc is given in the parenthesis. The result for $z = 3$ duty cycle scenario is given in parenthesis, because they are somewhat unreliable owing to small sample size.

Baugh, C. M., Lacey, C. G., Frenk, C. S., Granato, G. L., Silva, L., Bressan, A., Benson, A. J., & Cole, S. 2005, MNRAS, 356, 1191
Beckwith, S. V. W., Stiavelli, M., Koekemoer, A. M., Caldwell, J. A. R., Ferguson, H. C., Hook, R., Lucas, R. A., Bergeron, L. E., et al. 2006, AJ, 132, 1729
Bouwens, R. J., Illingworth, G. D., Blakeslee, J. P., & Franx, M. 2006, ApJ, 653, 53
Bouwens, R. J., Illingworth, G. D., Franx, M., & Ford, H. 2007, ArXiv e-prints, 707
Bouwens, R. J., Illingworth, G. D., Thompson, R. I., Blakeslee, J. P., Dickinson, M. E., Broadhurst, T. J., Eisenstein, D. J., Fan, X., et al. 2004, ApJL, 606, L25
Bruzual, G. & Charlot, S. 2003, MNRAS, 344, 1000
Bunker, A. J., Stanway, E. R., Ellis, R. S., & McMahon, R. G. 2004, MNRAS, 355, 374
Chary, R.-R. 2007, ArXiv e-prints, 712
Chen, H.-W., Prochaska, J. X., & Gnedin, N. Y. 2007, ApJ, 667, L125
Davé, R. 2007, ArXiv e-prints, 710
Davé, R., Finlator, K., & Oppenheimer, B. D. 2006, MNRAS, 370, 273
Davé, R., Hernquist, L., Katz, N., & Weinberg, D. H. 1999, ApJ, 511, 521
Dawson, S., Rhoads, J. E., Malhotra, S., Stern, D., Dey, A., Spinrad, H., Jannuzi, B. T., Wang, J., & Landes, E. 2004, ApJ, 617, 707
Di Matteo, T., Colberg, J., Springel, V., Hernquist, L., & Sijacki, D. 2007, ArXiv e-prints (0705.2269), 705
Di Matteo, T., Springel, V., & Hernquist, L. 2005, Nature, 433, 604
Dickinson, M., Stern, D., Giavalisco, M., Ferguson, H. C., Tsvetanov, Z., Chornock, R., Cristiani, S., Dawson, S., Dey, A., Filippenko, A. V., Moustakas, L. A., Nonino, M., Papovich, C., Ravindranath, S., Riess, A., Rosati, P., Spinrad, H., & Vanzella, E. 2004, ApJ, 600, L99
Dow-Hygelund, C. C., Holden, B. P., Bouwens, R. J., Illingworth, G. D., van der Wel, A., Franx, M., van Dokkum, P. G., Ford, H., et al. 2007, ApJ, 660, 47
Drory, N., Salvato, M., Gabasch, A., Bender, R., Hopp, U., Feulner, G., & Pannella, M. 2005, ApJ, 619, L131
Fardal, M. A., Katz, N., Gardner, J. P., Hernquist, L., Weinberg, D. H., & Davé, R. 2001, ApJ, 562, 605
Fardal, M. A., Katz, N., Weinberg, D. H., & Davé, R. 2007, MNRAS, 379, 985
Finlator, K., Davé, R., Papovich, C., & Hernquist, L. 2006, ApJ, 639, 672

Fontana, A., Salimbeni, S., Grazian, A., Giallongo, E., Pentericci, L., Nonino, M., Fontanot, F., Menci, N., Monaco, P., Cristiani, S., Vanzella, E., de Santis, C., & Gallozzi, S. 2006, A&A, 459, 745
Furlanetto, S. R., Schaye, J., Springel, V., & Hernquist, L. 2005, ApJ, 622, 7
Gawiser, E., Francke, H., Lai, K., Schawinski, K., Gronwall, C., Ciardullo, R., Quadri, R., Orsi, A., et al. 2007, ArXiv e-prints, 710
Gawiser, E., van Dokkum, P. G., Gronwall, C., Ciardullo, R., Blanc, G. A., Castander, F. J., Feldmeier, J., Francke, H., et al. 2006, ApJ, 642, L13
Gronwall, C., Ciardullo, R., Hickey, T., Gawiser, E., Feldmeier, J. J., van Dokkum, P. G., Urry, C. M., Herrera, D., et al. 2007, ApJ, 667, 79
Haiman, Z. & Hui, L. 2001, ApJ, 547, 27
Haiman, Z., Spaans, M., & Quataert, E. 2000, ApJ, 537, L5
Heckman, T. M. 2001, in Astronomical Society of the Pacific Conference Series, Vol. 240, Gas and Galaxy Evolution, ed. J. E. Hibbard, M. Rupen, & J. H. van Gorkom, 345
Hopkins, P. F., Cox, T. J., Keres, D., & Hernquist, L. 2007a, ArXiv e-prints, 706
Hopkins, P. F., Hernquist, L., Cox, T. J., & Keres, D. 2007b, ArXiv e-prints, 706
Hopkins, P. F., Hernquist, L., Cox, T. J., Robertson, B., & Krause, E. 2007c, ApJ, 669, 45
Hu, E. M. & Cowie, L. L. 2006, Nature, 440, 1145
Hu, E. M., Cowie, L. L., Capak, P., McMahon, R. G., Hayashino, T., & Komiyama, Y. 2004, AJ, 127, 563
Hu, E. M. & McMahon, R. G. 1996, Nature, 382, 231
Inoue, A. K., Iwata, I., & Deharveng, J.-M. 2006, MNRAS, 371, L1
Iwata, I., Ohta, K., Tamura, N., Akiyama, M., Aoki, K., Ando, M., Kiuchi, G., & Sawicki, M. 2007, MNRAS, 376, 1557
Kashikawa, N., Kitayama, T., Doi, M., Misawa, T., Komiyama, Y., & Ota, K. 2007, ArXiv e-prints, 704
Kashikawa, N., Shimasaku, K., Malkan, M. A., Doi, M., Matsuda, Y., Ouchi, M., Taniguchi, Y., Ly, C., et al. 2006, ApJ, 648, 7
Katz, N., Weinberg, D. H., & Hernquist, L. 1996, ApJS, 105, 19
Keel, W. C., Cohen, S. H., Windhorst, R. A., & Waddington, I. 1999, AJ, 118, 2547
Kennicutt, R. C. J. 1998, ApJ, 498, 541
Kobayashi, M. A. R., Totani, T., & Nagashima, M. 2007, ArXiv e-prints, 705
Kormendy, J. & Gebhardt, K. 2001, in AIP Conf. Proc., 20th Texas Symposium on Relativistic Astrophysics, ed. J. C. Wheeler & H. Martel, Vol. 586 (New York: Am. Inst. Phys.), 363
Kovač, K., Somerville, R. S., Rhoads, J. E., Malhotra, S., & Wang, J. 2007, ArXiv e-prints, 706
Lai, K., Huang, J.-S., Fazio, G., Cowie, L. L., Hu, E. M., & Kakazu, Y. 2007a, ApJ, 655, 704
Lai, K., Huang, J.-S., Fazio, G., Gawiser, E., Ciardullo, R., Damen, M., Franx, M., Gronwall, C., Labbe, I., Magdis, G., & van Dokkum, P. 2007b, ArXiv e-prints, 710
Landy, S. D. & Szalay, A. S. 1993, ApJ, 412, 64
Larson, R. B. 1998, MNRAS, 301, 569
Le Delliou, M., Lacey, C., Baugh, C. M., Guiderdoni, B., Bacon, R., Courtois, H., Sousbie, T., & Morris, S. L. 2005, MNRAS, 357, L11
Le Delliou, M., Lacey, C. G., Baugh, C. M., & Morris, S. L. 2006, MNRAS, 365, 712
Leitherer, C., Schaerer, D., Goldader, J. D., Delgado, R. M. G., Robert, C., Kune, D. F., de Mello, D. F., Devost, D., & Heckman, T. M. 1999, ApJS, 123, 3
Li, Y., Hernquist, L., Robertson, B., Cox, T. J., Hopkins, P. F., Springel, V., Gao, L., Di Matteo, T., Zentner, A. R., Jenkins, A., & Yoshida, N. 2007, ApJ, 665, 187
Madau, P. 1995, ApJ, 441, 18
Madau, P., Pozzetti, L., & Dickinson, M. 1998, ApJ, 498, 106
Malhotra, S. & Rhoads, J. E. 2002, ApJ, 565, L71
—. 2004, ApJ, 617, L5
Malhotra, S., Rhoads, J. E., Pirzkal, N., Haiman, Z., Xu, C., Daddi, E., Yan, H., Bergeron, L. E., et al. 2005, ApJ, 626, 666
Matsuda, Y., Yamada, T., Hayashino, T., Tamura, H., Yamauchi, R., Ajiki, M., Fujita, S. S., Murayama, T., et al. 2004, AJ, 128, 569
McQuinn, M., Hernquist, L., Zaldarriaga, M., & Dutta, S. 2007, MNRAS, 381, 75
Mori, M. & Umemura, M. 2006, Nature, 440, 644
Murayama, T., Taniguchi, Y., Scoville, N. Z., Ajiki, M., Sanders, D. B., Mobasher, B., Aussel, H., Capak, P., Koekemoer, A., Shioya, Y., Nagao, T., Carilli, C., Ellis, R. S., Garilli, B., Giavalisco, M., Kitzbichler, M. G., Le Fèvre, O., Maccagni, D., Schinnerer, E., Smolčić, V., Tribiano, S., Cimatti, A., Komiyama, Y., Miyazaki, S., Sasaki, S. S., Koda, J., & Karoji, H. 2007, ApJS, 172, 523
Nagamine, K., Cen, R., Hernquist, L., Ostriker, J. P., & Springel, V. 2004a, ApJ, 610, 45
—. 2005, ApJ, 627, 608
Nagamine, K., Ostriker, J. P., Fukugita, M., & Cen, R. 2006a, ApJ, 653, 881
Nagamine, K., Springel, V., & Hernquist, L. 2004b, MNRAS, 348, 435
Nagamine, K., Springel, V., Hernquist, L., & Machacek, M. 2004c, MNRAS, 350, 385
Nagamine, K., Wolfe, A. M., & Hernquist, L. 2006b, ApJ, 647, 60
Nagashima, M., Yahagi, H., Enoki, M., Yoshii, Y., & Gouda, N. 2005, ApJ, 634, 26
Night, C., Nagamine, K., Springel, V., & Hernquist, L. 2006, MNRAS, 366, 705
Oesch, P. A., Stiavelli, M., Carollo, C. M., Bergeron, L. E., Koekemoer, A. M., Lucas, R. A., Pavlovsky, C. M., et al. 2007, ArXiv e-prints, 706
Ouchi, M., Hamana, T., Shimasaku, K., Yamada, T., Akiyama, M., Kashikawa, N., Yoshida, M., Aoki, K., Iye, M., Saito, T., Sasaki, T., Simpson, C., & Yoshida, M. 2005a, ApJ, 635, L117
Ouchi, M., Shimasaku, K., Akiyama, M., Sekiguchi, K., Furusawa, H., Okamura, S., Kashikawa, N., Iye, M., Kodama, T., Saito, T., Sasaki, T., Simpson, C., Takata, T., Yamada, T., Yamanoi, H., Yoshida, M., & Yoshida, M. 2005b, ApJ, 620, L1
Ouchi, M., Shimasaku, K., Akiyama, M., Simpson, C., Saito, T., Ueda, Y., Furusawa, H., Sekiguchi, K., Yamada, T., Kodama, T., Kashikawa, N., Okamura, S., Iye, M., Takata, T., Yoshida, M., & Yoshida, M. 2007, ArXiv e-prints, 707
Ouchi, M., Shimasaku, K., Furusawa, H., Miyazaki, M., Doi, M., Hamabe, M., Hayashino, T., Kimura, M., Kodaira, K., Komiyama, Y., et al. 2003a, ApJ, 582, 60
Ouchi, M., Shimasaku, K., Furusawa, H., Miyazaki, M., Doi, M., Hamabe, M., Hayashino, T., Kimura, M., et al. 2003, ApJ, 582, 60
Ouchi, M., Shimasaku, K., Okamura, S., Furusawa, H., Kashikawa, N., Ota, K., Doi, M., Hamabe, M., Kimura, M., Komiyama, Y., Miyazaki, M., Miyazaki, S., Nakata, F., Sekiguchi, M., Yagi, M., & Yasuda, N. 2004a, ApJ, 611, 660
—. 2004b, ApJ, 611, 685
Partridge, R. B. & Peebles, P. J. E. 1967, ApJ, 147, 868
Peng, C. Y., Impey, C. D., Rix, H.-W., Kochanek, C. S., Keeton, C. R., Falco, E. E., Lehár, J., & McLeod, B. A. 2006, ApJ, 649, 616
Pentericci, L., Grazian, A., Fontana, A., Salimbeni, S., Santini, P., De Santis, C., Gallozzi, S., & Giallongo, E. 2007, ArXiv Astrophysics e-prints
Perez-Gonzalez, P. G., Rieke, G. H., Villar, V., Barro, G., Blaylock, M., Egami, E., Gallego, J., Gil de Paz, A., Pascual, S., Zamorano, J., & Donley, J. L. 2007, ArXiv e-prints, 709
Pettini, M. 2004, in Cosmochemistry. The melting pot of the elements, ed. C. Esteban, R. García López, A. Herrero, & F. a.-p. Sánchez, 257–298
Pettini, M., Rix, S. A., Steidel, C. C., Adelberger, K. L., Hunt, M. P., & Shapley, A. E. 2002, ApJ, 569, 742
Pettini, M., Shapley, A. E., Steidel, C. C., Cuby, J.-G., Dickinson, M., Moorwood, A. F. M., Adelberger, K. L., & Giavalisco, M. 2001, ApJ, 554, 981
Pirzkal, N., Malhotra, S., Rhoads, J. E., & Xu, C. 2007, ApJ, 667, 49
Rhoads, J. E., Malhotra, S., Dey, A., Stern, D., Spinrad, H., & Jannuzi, B. T. 2000, ApJ, 545, L85
Robertson, B., Hernquist, L., Cox, T. J., Di Matteo, T., Hopkins, P. F., Martini, P., & Springel, V. 2006, ApJ, 641, 90
Saito, T., Shimasaku, K., Okamura, S., Ouchi, M., Akiyama, M., Yoshida, M., & Ueda, Y. 2007, ArXiv e-prints, 705
Santos, M. R., Ellis, R. S., Kneib, J.-P., Richard, J., & Kuijken, K. 2004, ApJ, 606, 683
Schaerer, D. 2003, A&A, 397, 527
Shapley, A. E., Steidel, C. C., Adelberger, K. L., Dickinson, M., Giavalisco, M., & Pettini, M. 2001, ApJ, 562, 95

Shapley, A. E., Steidel, C. C., Pettini, M., & Adelberger, K. L. 2003, ApJ, 588, 65
Shimasaku, K., Hayashino, T., Matsuda, Y., Ouchi, M., Ohta, K., Okamura, S., Tamura, H., Yamada, T., et al. 2004, ApJ, 605, L93
Shimasaku, K., Kashikawa, N., Doi, M., Ly, C., Malkan, M. A., Matsuda, Y., Ouchi, M., Hayashino, T., et al. 2006, PASJ, 58, 313
Sijacki, D., Springel, V., Di Matteo, T., & Hernquist, L. 2007, ArXiv e-prints, 705
Springel, V. 2005, MNRAS, 364, 1105
Springel, V., Di Matteo, T., & Hernquist, L. 2005, ApJ, 620, L79
Springel, V. & Hernquist, L. 2002, MNRAS, 333, 649
—. 2003a, MNRAS, 339, 289
—. 2003b, MNRAS, 339, 312
Stanway, E. R., Bunker, A. J., McMahon, R. G., Ellis, R. S., Treu, T., & McCarthy, P. J. 2004, ApJ, 607, 704
Steidel, C. C., Adelberger, K. L., Shapley, A. E., Pettini, M., Dickinson, M., & Giavalisco, M. 2000, ApJ, 532, 170
Taniguchi, Y., Ajiki, M., Nagao, T., Shioya, Y., Murayama, T., Kashikawa, N., Kodaira, K., Kaifu, N., et al. 2005, PASJ, 57, 165
van Dokkum, P. 2007, ArXiv e-prints, 710
Vanzella, E., Cristiani, S., Dickinson, M., Kuntschner, H., Nonino, M., Rettura, A., Rosati, P., Vernet, J., et al. 2006, A&A, 454, 423
Venemans, B. P., Röttgering, H. J. A., Miley, G. K., Kurk, J. D., De Breuck, C., Overzier, R. A., van Breugel, W. J. M., Carilli, C. L., et al. 2005, A&A, 431, 793
Wilkins, S. M., Trentham, N., & Hopkins, A. M. 2008, ArXiv e-prints, 801
Yan, H. & Windhorst, R. A. 2004, ApJ, 612, L93
Yoshida, M., Shimasaku, K., Kashikawa, N., Ouchi, M., Okamura, S., Ajiki, M., Akiyama, M., Ando, H., et al. 2006, ApJ, 653, 988